UNIVERSIDAD DEL NORTE

Departamento de Ingeniería Mecánica

PhD THESIS

Andrés Felipe López Garcia

Effect of alcohol fumigation on diesel engine

Supervised by

John Ramiro Agudelo S.
Prof. Dept. Ingeniería Mecánica. Universidad de Antioquia

Lesmes Antonio Corredor M.
Prof. Dept. Ingeniería Mecánica. Universidad del Norte

November 2014

Para mi familia, mis abuelos y Lili

ACKNOWLEDGEMENTS

Author wish to thank Dr. John R. Agudelo and Dr. Lesmes Corredor for their guidance and valuable contribution as the advisors of this work.

Author wish to thank Colciencias for granting my graduate scholarship and for financing my stay at the Universidad de Castilla-La Mancha (Spain).

the Sostenibilidad program 2014-2015 of the Universidad de Antioquia for the financial support. The Committee for the development of the research of the Universidad de Antioquia (CODI) is also acknowledged for the financial support through the project CODI PRG13-2-04.

Thanks to the Gimel and GAIA research groups of the Universidad de Antioquia by their unvaluable support.

Professors Magín Lapuerta and Octavio Armas from Universidad de Castilla-La Mancha (Spain) are greatfully acknowledged by their support with PM oxidation reactivity and morphology measurements through the project REACTEC Ref. ENE2010-20768-C03-01.

Professor Helmer Acevedo of the Universidad Nacional de Colombia in Bogotá (Colombia) is gratefully acknowledged for the ELPI Dekati measurements.

Thanks to Marlon and to all my friends from the Universidad de Antioquia (GIMEL) for their wonderful support in the experiments and the great remembers of the “black faces” during PM collecting.

Finally the Colombian Petroleum Company (Ecopetrol) is acknowledged for supplying the ULSD fuel.

ABSTRACT

The depletable nature of fossil fuels, combined with their price volatility and high contamination of large urban centers have motivated the research of renewable fuels as partial or even total substitutes of conventional fossil fuel. In diesel engines, biodiesel, hydrotreated vegetable oils (*HVO*) and bio-alcohols have gained prominence. In this work 10% of ultra-low sulfur diesel (*ULSD*) was substituted in energy basis with sugar cane hydrous ethanol (*H-Et*) and n-butanol (*n-BU*) through an intake multipoint port electronic injection system on an automotive diesel engine operating under steady conditions.

This research was divided into four phases: i) design and manufacture of alcohol injection system, ii) performance evaluation, emission and combustion of diesel engine, iii) analysis of the reactivity to oxidation, the nanostructure and morphology of the particulate matter (PM) and iv) study of the biological activity of the soluble organic fraction of particulate matter emitted by this technique.

Both Alcohols increased the brake specific fuel consumption (bsfc) compared to ULSD. Brake thermal efficiency (bte) remained unchanged at high loads but at low load decreased drastically respect to ULSD, showing the necessity of reaching a minimum thermal condition of the engine to start spraying alcohols. Independent of engine operation mode, both alcohols exhibited higher premixed combustion peaks, longer start of combustion, lower bulk in-cylinder temperature, faster combustion and poorer combustion smoothness (CoV) in comparison with ULSD. In contrast to the ULSD and hydrated ethanol, n-butanol provided an unusual heat release peak (less than 2% of the total heat release) before the premixed combustion.

From the experimental work and engine technology, it can be concluded that both alcohols increased carbon monoxide (CO) and total hydrocarbons (THC) emissions; however nitrogen oxides (NOx) and PM emissions as well as the particle number concentration (PNC) were reduced in comparison with the ULSD. The magnitude of this variation was significantly affected by the engine operating mode. At low engine speed and high fuel-air ratio, hydrated ethanol exhibited the lowest PM and NOx emissions, but the opposite trend was observed at high engine speed and low equivalence ratio, where n-butanol behaved the best among all fuels. Although both alcohols reduced the PNC drastically, the average geometric diameter of these particles was similar to the ULSD.

The chemical composition, reactivity to oxidation, nanostructure and morphology of PM were performed using various analytical techniques such as thermogravimetry (TGA), Diffuse Reflectance Infrared Fourier Transform Spectroscopy (DRIFTS), X-ray diffraction (XRD), Raman spectroscopy, transmission electron microscopy (TEM) and scanning (SEM). Results showed that regardless the operating mode, PM produced by alcohols fumigation was more reactive to oxidation compared to ULSD, and followed the order H-Et > n-Bu > ULSD. This study also found that the reactivity of oxidation was affected by the chemical composition of PM, but not by its nanostructure. The nanostructure and morphology soot were not affected by engine load at constant engine speed.

Finally, regardless engine operating mode, the biological reactivity of the soluble organic fraction (SOF) contained in the PM of both alcohols was more genotoxic than ULSD. This may be a barrier for this technology due to negative impact on human health.

CONTENTS

CHAPTER I: INTRODUCTION

The finite reserves of oil, the high prices of fossil fuels and the restrictive requirements of emission standards have stimulated the use of renewable fuels and the research for technologies to improve internal combustion engines. Regarding to diesel engines, biomass-derived fuels such as: biodiesel, bioalcohols (mainly bioethanol), biomass-to-liquid, and hydrotreated vegetable oils (HVO), are being used as partial surrogates of conventional diesel fuel. In particular, bioalcohols are an attractive option because: they can be easily blended or injected into the engine, they can be produced through fermentation processes from a high variety of vegetable sources (or also, by conversion technologies such as biomass gasification plus catalysis), and finally, they contain a high share of oxygen, which has the potential to reduce particulate matter (PM) emissions [1]. The main researched techniques for the use of bioalcohols in diesel engines can be divided into four categories: alcohol-diesel blends, alcohol-diesel emulsions (using an emulsifier to prevent blend separation), alcohol fumigation in the intake port, and dual fuel injection where the diesel is the pilot fuel [2]. While alcohol fumigation can displace up to 50% of diesel energy demand, the dual injection can reach around 90%, and alcohol/diesel blends and emulsions about 25% [3].

The simplest method to use alcohols in the diesel engines is through blends. However there are some barriers still unsolved: i) not all alcohols can be easily blended with diesel fuel (methanol is not soluble or has very limited solubility in the diesel fuel [3]), ii) although diesel (or biodiesel)-alcohols reduce NO emissions, they may increase CO and THC emissions [4]; iii) anhydrous bioethanol leads to poor stability according to temperature and water and ethanol content in the blend, which promotes fuels separation; [5]; iv) the hygroscopic capacity of ethanol promotes corrosion of the injection system and the fuel tank [1, 6]; v) the ethanol-diesel blends have low lubricity as compared to pure diesel fuel [1], which is a concern for manufacturers of high pressure injection pumps [7]; vi) alcohols have very low cetane number that reduces the cetane level of the alcohol–diesel blend (~7 points for every 10% ethanol in diesel [8]) and vii) there are high alcohol losses due to its evaporation from the fuel tank [9].

A good option to avoid these problems is alcohol fumigation, which enables to supply alcohols through the intake port, to enrich the admission charge. This technique has some advantages such as: 1) high flexibility on diesel fuel substitution since it can switch from 0 to as much as 50% of alcohol replacement on an energy basis [10]; 2) In contrast with direct blending, this enables varying the amount of alcohol injected to match the actual engine requirement [11], 3) hydrous alcohols can be used [12-14], 4) simultaneous reduction of NOx and PM emissions [3, 15], 5) while the total number concentration of

particles decreases, the geometrical mean diameter is not affected [16] and 6) the evaporation losses are lower in comparison with alcohol-diesel blends. However, this technique faces some technical challenges such as 1) the probability of severe knock under high-load conditions due to the low cetane numbers of the alcohols [17] which limits the quantity of alcohol substitution [13, 18]; 2) the high heat of evaporation of alcohols may lead to ignition difficulties and high aldehyde emissions at cold start, warming up and low load operations [19-21], 3) although it has proven to reduce PM and NOx, this technique increases CO, THC [3, 15] and NO_2 emissions [16, 22, 23] and 4) this requires an additional fuel injection system and fuel tank adaptation.

There is also lack of knowledge about how alcohol fumigation affects the morphology and the chemical characteristics of the soot emitted by the engine, as well as its toxicology potential. The soot nanostructure and its reactivity affect the performance of diesel particulate filter (DPF), and its chemical composition provides valuable information of its potential hazards to human health. The understanding of these interactions enables automotive industries design properly after-treatment systems such as diesel particulate filters (DPF) since performance and lifetime (translated in terms of frequency of regeneration events) of these devices are affected by nanostructure and oxidative properties of the particles[24].

In this work was developed an electronic control unit for the alcohols fumigation, later different experiments were performed in some operation modes of diesel engine. Fig. 1 shows all analysis implemented with the fumigation, the research can be divided in three parts: i) performance, combustion and emissions, ii) morphology and nanostructure of particulate matter and iii) biology analysis of extractable organic fraction of particulate matter. The study was executed in the laboratory of thermal machines at the Universidad de Antioquia.

1.1. General Objective

Determine the impact on performance and emissions of a diesel engine operating with electronic multipoint injection of hydrated ethanol and n-butanol.

1.2 Specific Objectives

- Determine the performance, emissions and combustion when used alcohol fumigation

- Analisys the effect of using alcohol fumigation on the nanostructure and chemical composition of particulate matter.

- Evaluate the biological activity of the particulate material

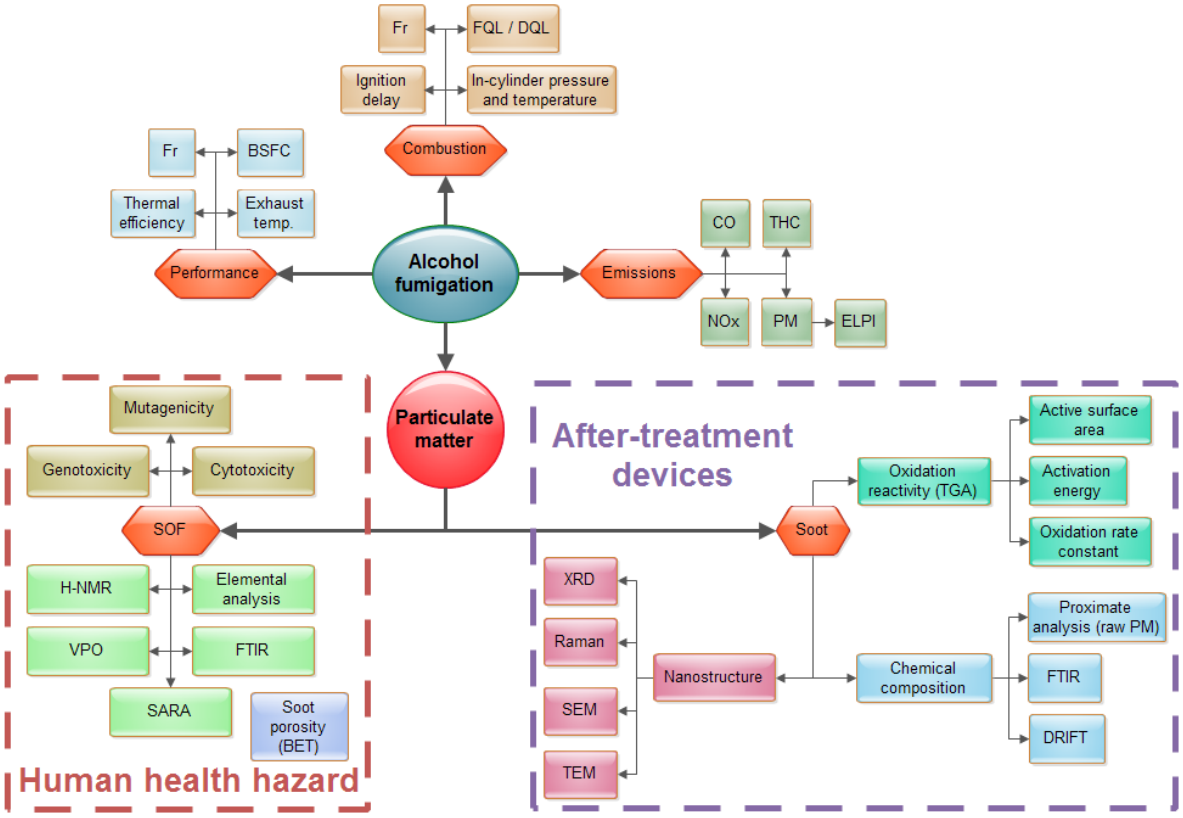

Fig. 1. Analysis performed in the research

CHAPTER II: Impact of n-butanol and hydrous ethanol fumigation on the performance and pollutant emissions of an automotive diesel engine[1]

John Agudelo[1,], Andrés López[1], Marlon Cadrazco[1], Andrés Agudelo[1], Lesmes Corredor[2], Juan Vélez[1]*

Keywords: n-butanol, hydrous ethanol, fumigation, diesel engine, particulate number

Highlights

- Hydrous ethanol and n-butanol were fumigated in an automotive diesel engine
- Alcohols led to lower in-cylinder pressure and temperature at all operating modes
- Alcohols exhibited poor engine performance and combustion at low loads
- Alcohols led to higher CO and THC and lower NOx, PM and particle number than ULSD
- Nano-size particulates of both alcohols were not smaller than ULSD fuel ones
- Butanol behave different than ethanol and were markedly affected by operating mode

2.1 Abstract

In this work an automotive diesel engine was modified with a built-in house multipoint port fumigation system to supply hydrous ethanol and n-butanol. Tests were carried out at three stationary engine operating modes in order to determine the impact of alcohols fumigation when fuel-air ratio and engine speed were varied. Alcohols were injected in the intake manifold just after the intake valve of every cylinder was opened in order to substitute 10% of ultra low diesel (ULSD) fuel in energy basis. Both alcohols increased brake specific fuel consumption (BSFC) in comparison with ULSD. Brake thermal efficiency (BTE) remained unchanged at high load, butdecreased drastically at low load, showing the necessity of a minimum engine thermal load to start alcohols fumigation. Independently of engine load and engine speed, both alcohols exhibited higher premixed combustion peaks, longer start of combustion, lower maximum in-cylinder temperature, faster combustion process and higher coefficient of variation of indicated mean effective pressure in comparison with ULSD. Different to ULSD and hydrous ethanol, n-butanol exhibited an atypical heat release (less than 2% of the total heat release) just before fast combustion period.

From this specific test conditions and engine technology it may be concluded that both alcohols increased CO and THC emissions, and simultaneously reduced NOx, sPM and particle number concentration compared to ULSD fuel, however the magnitude of this reduction was markedly affected by engine operating mode. At low engine speed and high

[1] This chapter has been submitted for publication at Fuel a journal from Elsevier

fuel-air ratio, hydrous ethanol exhibited lower sPM and higher specific NOx than n-butanol, however the contrary trend was observed at high engine speed and low fuel-air equivalence ratio. Finally, it is concluded that although both alcohols reduced drastically the PN concentration, the average geometrical diameter of these particulates was similar to ULSD fuel.

2.2 Introduction

The finite reserves of oil, the high prices of fossil fuels and the restrictive requirements of emission standards have stimulated the use of renewable fuels and the research for technologies to improve internal combustion engines. Biomass-derived fuels such as: biodiesel, alcohols (mainly bioethanol), biomass-to-liquid, and hydrotreated vegetable oils (HVO), are being used as partial surrogates of conventional diesel fuel. In particular, alcohols are attractive because: they can be easily blended or injected into the engine, they are produced through fermentation processes from a high variety of non-edible vegetable and organic waste sources, and finally, they contain a high share of oxygen, which has the potential to reduce particulate matter (PM) emissions [1]. The most popular techniques for using alcohols in diesel engines are alcohol-diesel blending and alcohol fumigation in the intake port [2]. While alcohol fumigation can replace up to 50% of conventional diesel in energy basis, alcohol-diesel blends can reach up to 25% [3].

Although alcohol blending is the easier method to implement, there are some challenges to be faced: i) some alcohols have poor solubility in diesel fuel (e.g., methanol [3]); ii) although diesel/alcohols or biodiesel/alcohols reduce NOx, they may increase CO and THC emissions [4]; iii) alcohols might cause poor stability depending on blend temperature [5]; iv) the hygroscopic capacity of some alcohols promotes corrosion in the injection system and the fuel tank [1, 6]; v) blends have less lubricity than diesel [1],[7]; vi) alcohols may reduce the cetane number of the blend (e.g., approx. 7 points for every 10% of ethanol in the blend [8]) and vii) high alcohol losses due to evaporation from the fuel tank [9].
A good alternative to avoid these problems is alcohol fumigation, which has the following advantages: i) high flexibility on diesel fuel substitution since it can switch from 0% to as much as 50% of alcohol replacement on an energy basis [10]; ii) the amount of alcohol injected can be adjusted to match the actual engine requirement [11], iii) hydrous alcohols can be used [12-14], iv) simultaneous reduction of NOx and PM emissions [3, 15], v) while the particle number concentration (PNC) decreases, the geometrical mean diameter is not affected [16] and vi) evaporation losses are lower in comparison with alcohol-diesel blends. However, this technique faces some disadvantages: a) possibility of severe knock under high-load conditions due to the low cetane numbers of the alcohols [17] which limits the quantity of diesel substitution [13, 18]; b) the high heat of evaporation of alcohols may lead to ignition difficulties and high aldehyde emissions at cold start, warm up and low load operations [19-21]; c) although it has proven to reduce PM and NOx, increases CO, THC

[3, 15] and NO_2 emissions [16, 22, 23] and d) requires an additional fuel injection system and fuel tank adaptation.

Alcohols fumigation was first addressed in 80´s decade. The most popular alcohol used for fumigation in diesel engines has been ethanol with different levels of water content, although methanol and n-butanol have also been studied. With regard to ethanol, Broukhiyan and Lestz [18] using an indirect injection diesel engine with fumigated anhydrous ethanol, observed modest improvements in thermal efficiency (except at low loads) and the maximum amount of substitution was limited by knocking. Additionally, for all operating conditions, ethanol fumigation reduced NOx and PM concentrations, but increased the biological activity of the particulates. Heisey and Lestz [12], fumigated hydrous ethanol (0% to 30% of water content by volume) on a single-cylinder, direct injection (DI) diesel engine and reported an increase in thermal efficiency, as well as in the ignition delay and CO emissions with respect to diesel fuel. Although PM decreased, its biological activity and the soluble organic fraction were increased for most operating conditions. They found that water content induced a higher NOx emissions reduction in comparison with the results reported in [18] with anhydrous ethanol. Hayes et al [12-14] found that high water content ethanol fumigation (25% to 50 %) resulted in larger NO reduction, lower peak pressures and rates of pressure rise in comparison with low water content ethanol (0% to 25%).

Goering et al [25], used a venturi-type carburetor to fumigate hydrous ethanol (40% and 50% of water content by vol.) in a naturally-aspirated diesel engine, showing that ethanol is completely vaporized only if the air was preheated. Ajav et al [26] using an stationary diesel engine found that, although the preheating approach improved the vaporization of hydrous ethanol (3% of water by vol.), there was a decrease in power output due to lower charge density. Abu-Qudais et al [10] found that diesel optimal substitutions were 20% for ethanol fumigation and 15% for e-diesel blends in a variable compression, single cylinder diesel engine. The fumigation produced an increase of 7.5% in thermal efficiency (3.6% for e-diesel), 55% in CO emissions (43.3 for e-diesel), 36% in THC emissions (34.4% for e-diesel) and a reduction of 51% in soot mass concentration (32% for e-diesel) with respect to conventional diesel.
Lu et al [27], using a single cylinder diesel engine operating with biodiesel observed that the amount of fumigated anhydrous ethanol delayed the start of combustion significantly, and the premixed heat release phase was increased smoothly. Also, they showed that NOx and smoke opacity were reduced simultaneously between 35-80% compared to neat biodiesel, while CO and THC concentrations were increased. Rodriguez-Fernandez et al [28], fumigated anhydrous ethanol in a single cylinder naturally aspirated diesel engine operating with ULSD or gas-to-liquid (GTL) and found that in both cases, ethanol decreased NOx and smoke emissions, but increased THC and CO; however the reduction was greater when the engine was run with GTL.

Surawski et al, [29] using a diesel engine fumigated with anhydrous ethanol showed that the reduction in particle size, the increased volatility, and the increase in potential particle toxicity of ethanol with respect to conventional diesel could be a barrier for this technology. Surawski et al [30], under the same experimental setup, also reported reductions in NO and PM2.5 emissions, and significant increases in CO, THC and PNC in most engine operating modes.

With regard to fumigation with methanol, several researchers agree that it increases THC, CO, and NO_2, and decreases NOx, smoke opacity, and PM [19-21, 31]. Zhang et al [32] showed that maximum cylinder pressure decreases at low/medium engine loads but increases at high engine loads. Methanol increased peak heat release rate and ignition delay but did not significantly change combustion duration. Additionally, a significant decrease in PM and PNC was observed at medium/high engine loads.
With respect to fumigation with n-butanol, Michikawauchi et al. [33] used a Euro 5 diesel engine to compare fumigation against a n-butanol-diesel blend under two conditions: constant thermal efficiency and constant NOx emissions. They found that at constant thermal efficiency, the fumigation was more effective at reducing NOx emissions than blending, (-43% *vs* -40% at high load and -73% *vs* -50% at middle load). At constant NOx and low load, thermal efficiency of both techniques decreased (-0.6% for fumigation *vs* -1.0% for blending), while THC emissions increased (400 % for fumigation *vs* 150% for blending). Soloiu et al. [34] investigated the port fuel injection of n-butanol combined with the direct injection of biodiesel to attain premixed homogeneous charge compression ignition (PCCI) for low-emissions at idling operation in an experimental single-cylinder DI diesel engine. They reported a maximum reduction of 98% of soot and 75% of NOx at 3 bar IMEP. However, CO and THC emissions increased from 10 to 20 times in comparison with diesel fuel depending on engine speed and load.

Chen et al. [35, 36] used a single-cylinder DI diesel engine operated with 15% and 45% EGR rates to compare n-butanol fumigation against a n-butanol-diesel blend. They found that n-butanol fumigation in combination with EGR could simultaneously reduce both NOx and soot emission to a very low level, but increased the indicated specific fuel consumption and decreased the indicated thermal efficiency. Compared with the blend, the n-butanol fumigation exhibited higher THC and CO emissions and lower thermal efficiency. Liu et al. [37] fumigated n-butanol on a modified heavy duty single-cylinder diesel engine fuelled with soybean oil biodiesel. Results indicated that very low NOx and soot emissions can be achieved simultaneously, but the increase of n-butanol fumigation ratio produced higher THC and CO emissions in comparison with neat biodiesel. They also detected a knocking limit at high load for high n-butanol substitution.

In summary, from the literature review it can be concluded that alcohols fumigation: i) increases fuel consumption due to the lower energy content of alcohols, ii) promotes knocking at high substitution levels due to alcohols lower cetane number, iii) increases CO and THC emissions due to the combination of the decrease of in-cylinder temperature and the adsorption of alcohols in the lubricating oil layers, although they can be drastically reduced by using a diesel oxidation catalyst [16], iv) reduces NOx emissions due to lower in-cylinder average bulk temperature induced by alcohols evaporation, v) reduces PM due to the additional oxygen in alcohols and to the decrease of aromatic and sulfur share of the diesel fuel, vi) there is not enough research on the effect of fumigation on the PNC and particulate size and vii) there is also lack of knowledge on the variation of engine operating mode with different alcohols.
Based on the previous summary, this work aims to analyze the impact of hydrous ethanol and n-butanol fumigation on the performance, combustion, pollutant emissions and particle number concentration and size of an automotive diesel engine at three operating modes. Hydrous ethanol was selected due to its low price and worldwide availability, and n-butanol because it is a promising renewable alcohol that can be obtained from biomass residues.

2.3 Methodology

2.3.1 Engine test rig

The schematic of the engine setup is presented in Fig. 2. Experiments were carried out in a 4-cylinder, 2.5l, turbocharged, DI automotive diesel engine (Table 1) which was modified with a built-in house intake multipoint port injection system (*Fig. 3*) to substitute 10% of diesel fuel on energy basis by hydrous ethanol (H-Et10) and n-butanol (n-Bu10). The engine was coupled to a Schenck W230 eddy current dynamometer. The air consumption was measured with a Magnetrol TA2 hotwire sensor, and diesel and alcohol flows were measured with two separate Shimadzu electronic weight scales (±0.01 g). The instantaneous in-cylinder pressure was recorded with a Kistler 6056A piezoelectric pressure transducer coupled to a Kistler 5011B charge amplifier. The instantaneous piston position was measured with a Heidennhain ROD 426 angular encoder of 1024 pulses/rev. High speed data were acquired using the Labview™ software and a National Instruments™ data acquisition system (NI PCI 6024E and NI PCI MIO-16E-4).

A zero-dimensional, one-zone thermodynamic combustion diagnosis model [38], based on in-cylinder pressure signal was used. A total of 100 pressure curves were registered at each operation mode to ensure reliability in the combustion diagnosis results. CO and NOx emissions were measured with an AVL Dicom 4000 NDIR sensor and total hydrocarbons (THC) emissions were recorded with a ThermoFID 2000e flame ionization detector through a heated line (190 °C). The size and number of PM were measured with a Dekati Electrical Low Pressure Impactor (ELPI) provided with a double diluter. Specific PM was obtained with a dilution rate of 10 through a Ricardo partial dilution tunnel. Whatman

microfiber glass filters of 47 mm diameters were conditioned to 22 °C and 45% humidity for 48 h before and after PM collecting procedure. A Shimadzu high precision weight scale (±1x10-5 g) was used to determine the collected mass of PM.

Table 1 Automotive diesel engine characteristics

Reference	Isuzu 4JA1
Type	4 in-line cylinders, 4-stroke, Turbocharged, DI, rotary pump
Swept volume (cm^3)	2499
Bore x stroke (mm)	93 x 92
Compression ratio	18.4
Inlet valve closure	54.5 c.a. deg.
Exhaust valve opening	55.5 c.a. deg.
Rated power	59 kW at 4100 min^{-1}
Maximum torque	170 Nm at 2300 min^{-1}

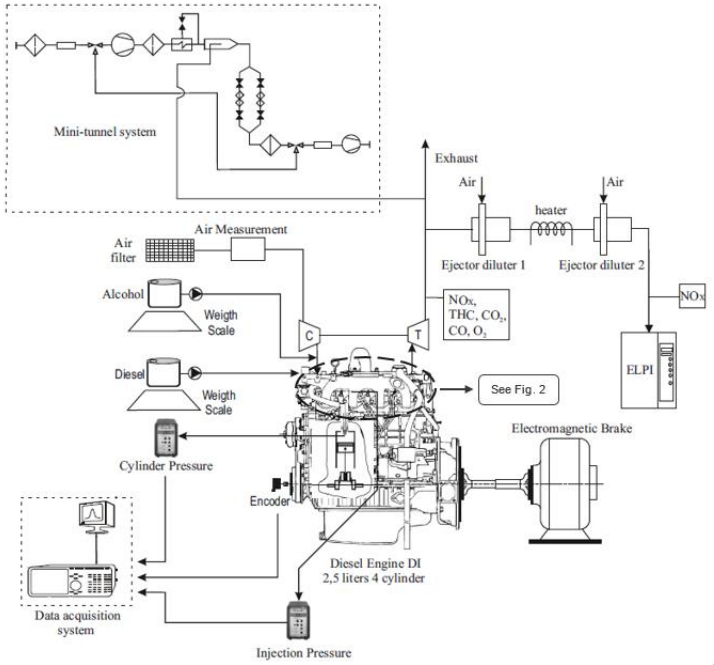

Fig. 2. Experimental setup

Fig. 3. Intake multipoint port injection (IMPI) system

2.3.2 Electronic fumigation system

Each alcohol was injected at a pressure of 300 kPa. The needle lift of each injector was controlled with a built-in house electronic control unit which was programmed in a Freescale™ microcontroller using Labview™ software. To ensure the synchronization of the alcohol injection timing, a proximity sensor was installed in the intake valve of cylinder

#1. An engine speed sensor of 60 pulses per revolution was also implemented. Both sensors were connected to the microcontroller, which was programmed to configure and manage the alcohol injection process. The algorithm first configures the initial parameters for the correct operation of the microcontroller and then sets the injector opening time from the Labview-based software. Afterwards, the algorithm locates the intake top dead center (TDC) of cylinder #1 in order to synchronize the injection process of all alcohol injectors, which followed the order 2-3-4-1, and calculates the injection duration (ms) according to the set point established by the user (open loop).

The duration of the intake stroke in a complete thermodynamic cycle (two engine revolutions) at 2410 min^{-1} (or 40.16 s^{-1}) is 24.89 ms (or 1000/40.16 ms). This means that the available time for alcohol injection is 12.45 ms (or 24.89/2 ms). Calculations established that alcohol droplets move from the injector nozzle to the intake valve in 4 ms. Considering this, the alcohol injector can be opened for up to 8.45 ms, to assure that the alcohol enters into the cylinder during intake stroke. Injection duration was set to around 2 ms for mode M4 and about 4 ms for mode M2.

2.3.3 Design of experiments and repeatability tests

The following engine operating modes were selected (Fig. 4): M1 (4.78 bar of brake mean effective pressure -bmep- at 1890 min^{-1}), M2 (4.78 bar of bmep at 2410 min^{-1}) and M4 (2.16 bar of bmep at 2410 min^{-1}). M2 was selected because it was the point of minimum air–fuel ratio and maximum smoke opacity according to the FTP75 homologation cycle (obtained by means of vehicle dynamics analysis) [39] Modes M1 and M4, were selected in order to determine the impact of alcohol type and engine load (M2 *vs* M4) and to establish the impact of alcohol type and engine speed (M1 *vs* M2) on fuel-air equivalence ratio, brake specific fuel consumption (bsfc), brake thermal efficiency (bte), relevant combustion parameters and pollutant emissions. Tests were carried out under carefully controlled conditions, in such a way that the difference in performance and pollutant emissions could be attributed only to differences in fuel properties and engine operating mode. To avoid dispersion of the results, the exhaust gas recirculation (EGR) valve was closed.

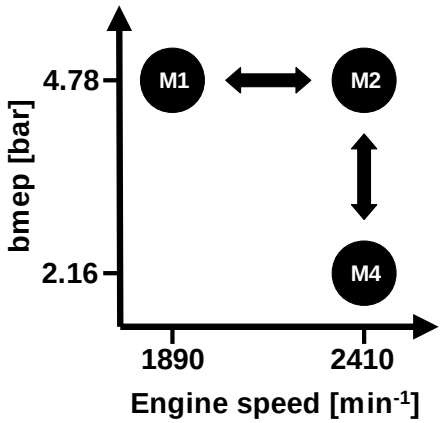

Fig. 4. Engine operating modes

A repeatability study of the test rig was carried out using ultra-low sulfur diesel (ULSD) fuel. A set of 12 measurements were conducted during several days and different climate conditions. The uncertainty of the computed results was lower than its standard deviation (Table 2). A 95% reliability level was reached by this repeatability study.

Table 2 Repeatability study of the test

Parameter	Units	Measure	Uncertainty (± abs.)
Engine speed	min^{-1}	2410	5
Torque	Nm	43	1
Mass flow of fuel	mg/s	895.9	0.1
Volumetric flow of air	m^3_n/h	94.44	0.01
Accuracy of calculated parameters			
Engine power	kW		± 0.275
Brake specific fuel consumption (bsfc)	g/kWh		± 7.6
Fuel-air ratio (F/A)	-		± 5.7 x 10^{-6}
Brake thermal efficiency (bte)	%		± 0.74

2.3.4 Fuel properties

Hydrous ethanol (H-Et) was obtained from a local sugar cane alcohol producer (92.56 % vol.); chemical grade (99.9%) n-Butanol (n-Bu) was provided by a local distributor. The reference fuel was ULSD, supplied by the Colombian petroleum company (Ecopetrol) (Table 3).

Table 3 Properties of ULSD, H-Et (94.16% w/w purity) and n-Bu (99.9 % w/w purity)

Fuel properties	ULSD	Hydrous ethanol	n-Butanol [40]
Chemical formula	$C_{14.7}H_{28.8}$	$C_{1.726}H_{5.452}O$	$C_4H_{10}O$
Fuel/Air ratio (stoichiometric)	1/14.7132	1/8.4651	1/11.1779
Density @ 15 ºC (kg/m^3)	856 [a]	809 [a]	810
Kinematic viscosity @ 40 ºC (cSt) [a]	3.625	1.454	2.500
Surface tension @ 25ºC (mN/m^{-1})	27.3 [41]	22.35 [42]	24.18 [43]
Cetane number	49	8	25
Lower heating value (kJ/kg) [a]	42,837	25,235	33,100
Molecular weight (kg/kmol)	205.2 [c]	42.2	74.0
Oxygen content (% weight)	0.0 [d]	37.9	21.6
C/H ratio	0.51 [d]	0.32	0.40
Sulfur content (ppm)	<15 [d]	0	0
Water content (% vol.)[a]	< 0.02	5.84	-
Latent heat of evaporation (kJ/kg)	265	948 [44]	585
Boiling point (°C)	202-362.5 [a]	77	118
Thermal conductivity (W/ m-K)[b]	-	0.165	0.153
Thermal diffusivity (Pa-s)[b]	-	0.123	0.091

[a] Measured, [b] Calculated, [c] Measured by vapor pressure osmometry (VPO), [d] Measured by elemental analysis (CHNOS)

2.4 Results and discussion

2.4.1 Impact of alcohol type and engine operating mode on combustion characteristics

The thermodynamic combustion diagnosis obtained from instantaneous in-cylinder pressure is shown in Fig. 5 and main combustion parameters are presented in Table 6 (hydrous ethanol data was not available at mode M1 due to problems with the in-cylinder instrumentation during experimentation). Mean in-cylinder pressure decreased with alcohol fumigation in comparison with ULSD at all engine operating modes (Fig. 5 top row) most likely due to the cooling effect of alcohols heat of evaporation (Table 3). Additionally the maximum in-cylinder pressure remained almost the same for both alcohols at all engine operating modes (Table 4), and the highest decrease (about 7% less than ULSD) was at mode M4, which could be due to the low temperature and low pressure inherent to this operating mode.

The bulk in-cylinder temperature decreased with the fumigation with respect to ULSD at all modes (Fig. 5 middle row) which could also be related to the cooling effect of alcohols latent heat. Fumigation did not alter the crank angle of maximum temperature in comparison with ULSD. During compression n-butanol exhibited the lowest bulk temperature among the fuels tested. This outcome was unexpected since n-butanol has

lower heat of evaporation (almost 50% less) and higher viscosity than hydrous ethanol (Table 3). At this point the reason for this result is unknown.

Both alcohols exhibited higher premixed combustion peaks at all engine operating modes compared to ULSD(Fig. 5 bottom row), this behavior was explained by Lu et al. [27] based on the lower cetane number of alcohols. Contrary to ULSD and hydrous ethanol, n-butanol showed a positive heat release rate just before the premixed combustion phase at M2 and M4, but not at M1. The higher cetane number of n-butanol (compared to ethanol) promoted its early autoignition at M2 and M4, given that both modes exhibited higher compression pressure and temperature in comparison with M1. At mode M1, with slightly lower compression pressure and temperature, the ignition delay was long enough for the n-butanol to be ignited by ULSD when injected (Table 4), Hydrous ethanol did not exhibit autoignition at any mode, due to its low cetane number. It is hypothesized that the early n-butanol heat release induced higher premixed combustion peak and higher maximum temperature in comparison with hydrous ethanol.

Cool-flames (low temperature combustion -LTC-) were not observed for n-butanol in this work likely due to: i) low cetane number of n-butanol, ii) the injection timing was not modified (advanced) and iii) the EGR was deactivated. This was in agreement with Zhang and Boehman [45] who reported that no noticeable low temperature heat release behavior was observed from the oxidation of neat n-butanol under diesel like conditions (modified CFR motored engine). Additionally, they found that n-butanol was consumed mainly through H-atom abstraction. Also Dagaut et al, using a detailed chemical kinetic mechanism, showed that n-butanol oxidized primarily through the abstraction of H-atoms on α-, β- and γ-carbon atoms of n-butanol followed by β-scission of the resulting radicals [46, 47]. Nevertheless, Soloiu et al. [34] achieved LTC through premixed charge compression ignition (PCCI) of n-butanol only at idle and low engine load of 1-3 bar IMEP, by controlling the intake port fuel mass flow rate and by advancing n-butanol injection timing, which led to longer premixing time resulting in a lean mixture and lower flame temperatures. This was not the case of the present study, since n-butanol was injected just when the intake valve was opened as commented before in section 2.3.2

As an indicator of combustion smoothness according to [27], the calculated coefficient of variation of *imep* for each fuel (COV, seeTable 4) displayed the following order: *hydrous ethanol* > *n-butanol* > *diesel*. This means that both alcohols induced higher combustion instabilities in comparison with ULSD operation, although they were below the 10% threshold [47]. Alcohols higher COV (compared to ULSD) could be a consequence of higher premixed combustion peaks, which result in higher pressure gradients that generate larger *imep* variations from cycle to cycle. Both alcohols showed the same order of COV (around 3% at mode M2 and around 5% at mode M4). Mode M4 presented higher COV than M2 for all fuels due to higher combustion instabilities under low temperature conditions.

In summary, independently of engine load (fuel-air ratio) and engine speed (combustion characteristic time), both alcohols exhibited higher premixed combustion peaks, lower

maximum in-cylinder temperature, faster combustion process and higher COV of imep in comparison with ULSD. The n-butanol exhibited an atypical heat release (1.9 % at mode M4 and 1.01% at mode M2 of the total heat release) just before premixed combustion period which was related with the ignition delay.

Table 4 Combustion results

Parameter	M1			M2			M4		
	ULSD	n-Bu10	H-Et10	ULSD	n-Bu10	H-Et10	ULSD	n-Bu10	H-Et10
Maximum in-cylinder average pressure [bar]	89.1	86.2 (-3.3%)[+]	N/A[*]	87.1	86.9 (-0.2%)	86.6 (-0.6%)	70.6	65.5 (-7.2%)	65.6 (-7.1%)
Maximum in-cylinder average temperature [K]	1403	1313 (-6.4%)	N/A	1583	1519 (-4.0%)	1563 (-1.3%)	1329	1249 (-6.0%)	1212 (-8.8%)
Coefficient of variation of imep	1.03	1.93 (87.4%)	N/A	0.95	3.18 (234.7%)	3.24 (241.1%)	2.29	4.89 (113.5%)	5.13 (124.0%)
Start of combustion [deg BTDC]	-10.33	-10.33 (0%)	N/A	-8.99	-8.99 (0%)	-8.63 (-4.0%)	-6.52	-4.41 (-32.4%)	-5.12 (-21.5%)

[*] N/A: not available data due to problems with in-cylinder instrumentation during this specific operating mode.

[+] Values indicate the percentage of variation with respect to ULSD

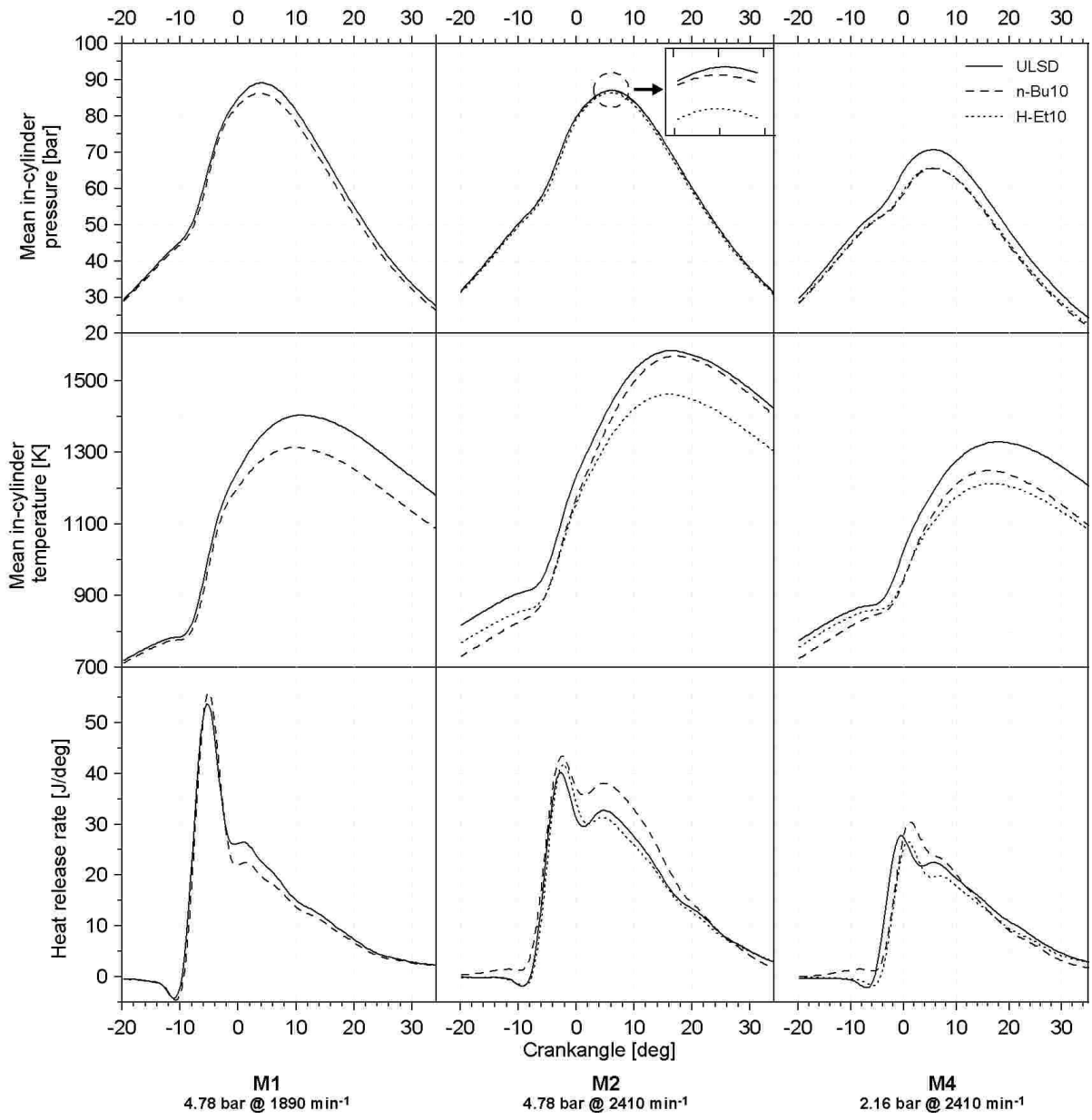

Fig. 5. Thermodynamic combustion diagnosis

2.4.2 Impact of alcohol type and engine operating mode on engine performance

Fuel-Air equivalence ratio (φ) did not change significantly for alcohols in comparison with ULSD at high load (M1 and M2). This is explained by the fact that the alcohol oxygen content balances the additional fuel required to compensate the 10% of ULSD in energy basis (due to the alcohol lower heating value). However, at low load (M4) φ increased about 30% for both alcohols (Fig. 6 top) with respect to ULSD due to lower in-cylinder temperature conditions. This is in agreement with Britto and Martins [48] who reported similar trends with ethanol fumigation. Finally, since hydrous ethanol has more oxygen

content and lower heating value than n-butanol, the fuel-air equivalence ratio remained almost the same for both alcohols at all operating modes

The brake specific fuel consumption (bsfc) increased as the lower heating value of the tested fuels decreased (Fig. 6. middle- and

Table 5) at all operating modes.

The remarkable increase of *bsfc* for both alcohols at low load (19.9% for n-Bu and 28% for H-Et) may be induced by the adverse conditions for alcohol evaporation due to lower engine thermal loads at mode M4.

The Brake thermal efficiency (bte, Fig. 6 bottom- and

Table 5) was not affected by fumigation at high engine loads, possibly due to the faster combustion induced by alcohol molecular oxygen content. Nevertheless, bte decreased at low load 13.2% for n-butanol and 15.2% for hydrous ethanol in comparison with ULSD. The poorer combustion of alcohol fumigation at low engine loads has been explained in [15]. who argued that the combination of the lower temperature (due to the cooling effect of alcohols) and the leaner fuel-air ratio, impact negatively the combustion process. Hydrous ethanol performed worse in comparison with n-butanol at M4 mode, probably due to the enthalpy of vaporization of the water.

In summary, the performance parameters were more affected by engine load (M2 vs M4) than by engine speed (M1 vs M2). Both alcohols performed better at high load compared to low load (where the alcohol fumigation drastically decreased bte and increased bsfc and φ). Therefore, it is recommendable to determine the specific thermal conditions for implementing fumigation strategy. None of the alcohols performed better than diesel, however, n-butanol performed better than hydrous ethanol, which showed the highest bsfc and the lowest bte among all fuels.

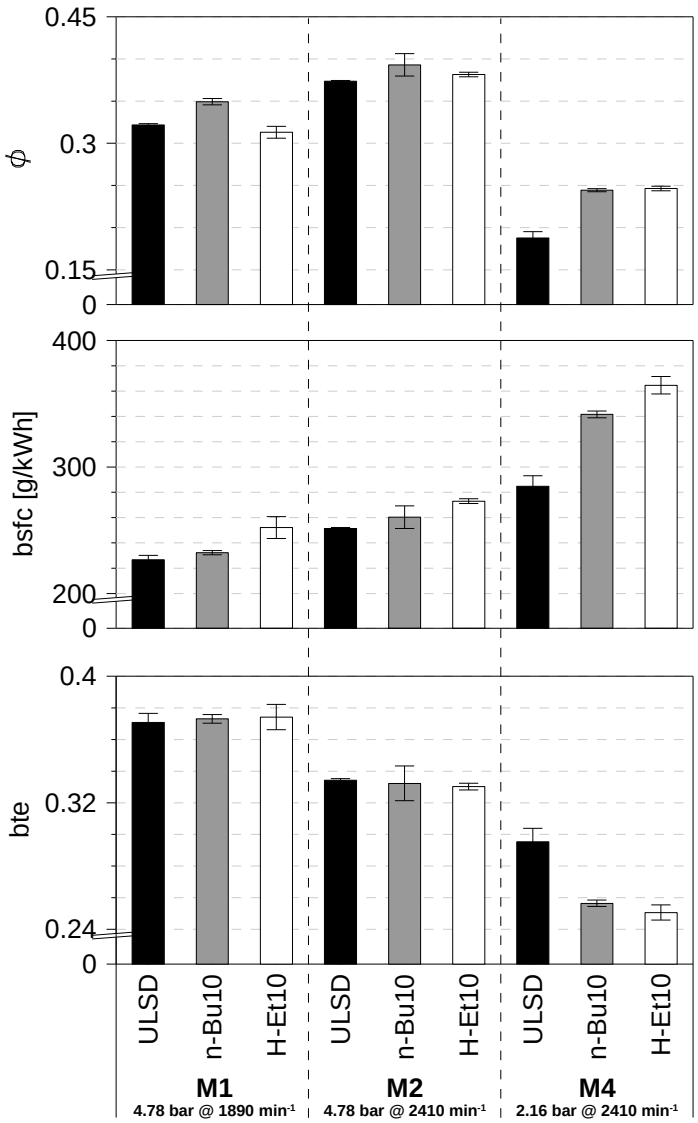

Fig. 6. Performance parameters for all engine operating modes and fuels

2.4.3 Impact of alcohol type and operating mode on pollutant emissions

Specific pollutant emissions and their percent changes compared to ULSD fuel are shown in Fig. 7 and Table 5 respectively. The CO produced by both alcohols (see Fig. 7-first row-) followed the trend: M2 < M1 < M4 probably due to the decreasing tendency shown in-cylinder bulk temperature (see Fig. 5). However with respect to ULSD, fumigation generated higher CO emissions for all engine modes as widely reported by other authors. CO increase has been explained by the combination of: i) partial fuel oxidation due to low in-cylinder bulk average temperature (Fig. 5-middle row-), ii) incomplete combustion of alcohols resulting from air/alcohol mixture trapped in crevices and iii) insufficient evaporation of alcohol liquid droplets adhered to oil layer in the chamber walls. M1 was the mode with the highest percent change of CO emissions in comparison with ULSD (~900% for n-butanol and ~1260% for hydrous ethanol). Similar orders of magnitude have been

obtained by other researchers (~800% with hydrous ethanol by Baranescu et al.[13] and ~450% with methanol by Zhang et al [21].
The results obtained at M1 could be explained by the reduction in turbulence associated with lower engine speed, which may have affected mixture formation. Additionally, when comparing alcohols against each other, at high engine speed (M2 and M4) hydrous ethanol exhibited lower CO emissions than n-butanol, likely due to the fact that ethanol has a smaller C/H atom ratio and higher oxygen content (Table 3), which plays a major role in the CO-to-CO_2 conversion. In contrast, ethanol generated higher CO emissions than n-butanol at low engine speed (M1). Given that the hydrous ethanol bulk temperature data was not available, an explanation for this behavior at this point cannot be given.
As expected THC emissions (see Fig. 7-second row-) followed similar patterns as the ones described above for CO. This is due to the fact that CO and THC emissions are driven by the same physical phenomena affecting the oxidation, combustion and evaporation explained in the previous paragraph. However, when comparing alcohols, n-butanol always produced fewer THC emissions than hydrous ethanol across all engine modes. This behavior might be occurring due to the significant differences in the alcohols cetane number (Table 3).
For all fuels, NOx emissions (see Fig. 7-third row-) followed the order M1 > M2 > M4, decreasing inversely with speed (M1 vs M2) and decreasing with load (M2 vs M4). This decreasing trend is in agreement with the behavior of the premixed peak of heat release rate across engine modes (Fig. 5-bottom row-). With respect to ULSD, both alcohols also reduced NOx emissions (see

Table 5. Percent changes in performance and pollutant emissions compared to ULSD fuel). This is commonly explained by the relatively low in-cylinder bulk temperature promoted by the enthalpy of vaporization of alcohols (Table 3). When comparing alcohols, hydrous ethanol produced higher NOx emissions than n-butanol at high speed (M2 and M4), most likely due to the higher gradient of bulk in-cylinder temperature (see Fig. 5-middle row-). At low speed this tendency was inverted, and since there is no sufficient in-cylinder experimental data available for hydrous ethanol, this cannot be explained at this point.
For all fuels, PM emissions increased with speed (M1 vs M2) and with load reduction (M2 vs M4), following the order: M1 < M2 < M4 (see Fig. 7-bottom row-). The highest emission of PM, obtained at low load, can be explained due to the lowest in-cylinder temperature and lowest *bte* across engine modes. The PM reduction with engine speed (between M2 and M1) is most likely related to the combination of a reduction in fuel-air equivalence ratio and an increase in *bte*. For all engine modes, fumigation with both alcohols obtained lower PM emissions than ULSD. At high loads n-butanol emitted less PM than ethanol, in comparison with ULSD (

Table 5), possible due to ethanol water content. This trend was reversed at low load, probably due to ethanol higher molecular oxygen content which promoted higher PM oxidation

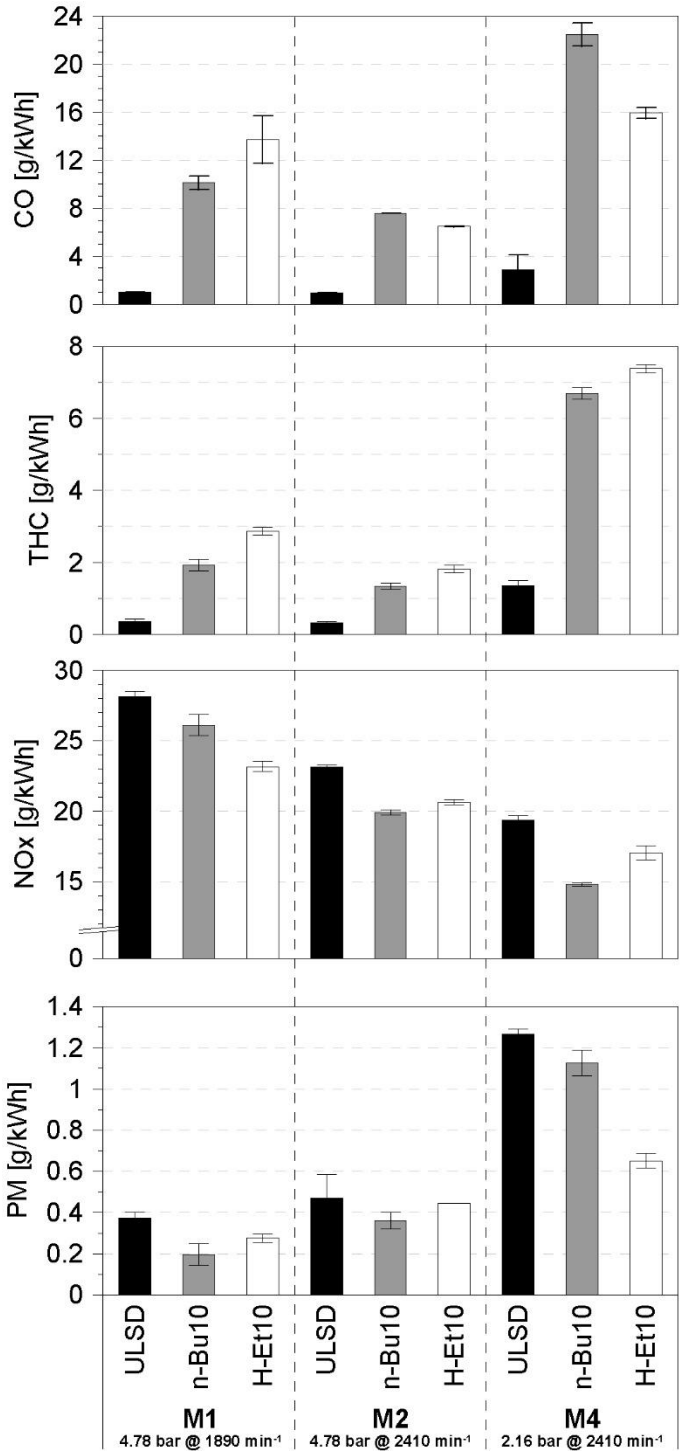

Fig. 7 Specific emissions

Table 5. Percent changes in performance and pollutant emissions compared to ULSD fuel

Mode	Fuel	φ	bsfc	bte	CO	THC	NOx	PM
M1 (4.78 bar @ 1890 min^{-1})	n-Bu	8.62	2.46	0.60	901.83	434.01	*-7.31*	*-47.38*
	H-Et	*-2.65*	11.24	0.90	1258.31	694.09	*-17.78*	*-26.05*
M2 (4.78 bar @ 2410 min^{-1})	n-Bu	5.19	3.55	*-0.62*	683.57	309.59	*-14.13*	*-23.27*
	H-Et	2.12	8.58	*-1.23*	570.47	456.11	*-10.93*	*-5.49*
M4 (2.16 bar @ 2410 min^{-1})	n-Bu	30.18	19.94	*-13.17*	684.70	390.86	*-23.66*	*-11.09*
	H-Et	31.26	28.02	*-15.15*	456.75	441.32	*-12.05*	*-48.49*

Fig. 8 shows the trade-off between NOx and PM emissions for all test conditions. While mode M1 exhibited the lowest PM and the highest NOx emissions, the contrary was observed for mode M4. With respect to ULSD, both alcohols reduced specific NOx and PM emissions for all engine operating modes, although the magnitude of reduction was markedly affected by engine operating mode. Hydrous ethanol showed lower PM and higher specific NOx than n-butanol at low engine speed and high fuel-air ratio (M1) and the reverse trend was observed at mode M4 (high engine speed and low fuel-air equivalence ratio). In conclusion, n-butanol showed the best trade-off because it exhibited the lowest NOx and the lowest PM emissions among all fuels.

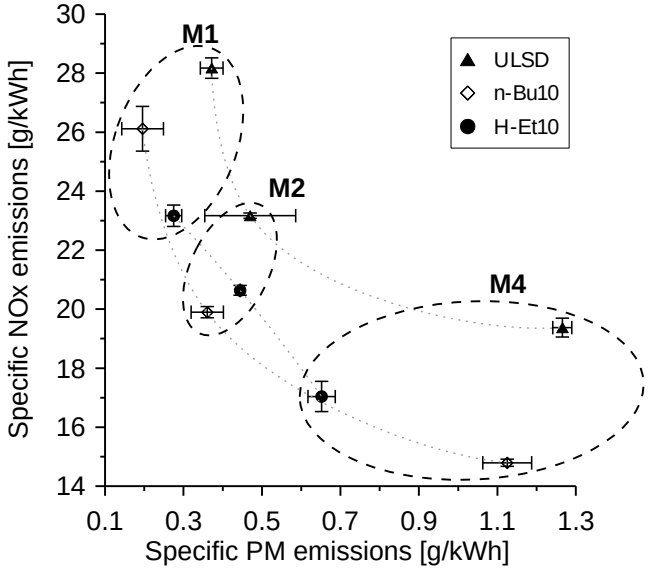

Fig. 8. Effect of alcohol fumigation on NOx-PM trade-off

Fig. 9 shows that total particulate number (PN) concentration, as obtained with the ELPI, was drastically reduced for both alcohols in all cases compared with ULSD fuel. PN

concentration was not shift toward smaller or higher particulate geometric diameters. This result is in agreement with the work of Yao et al. [49] and Zhang et al. [11] who showed that ethanol fumigation induced a reduction of total PN concentration, without significant changes of the diameter of the particulates. Alcohol fumigation, especially n-butanol, showed a drastic decrease in the number of nano-sized particulates (10 nm < D_i < 30 nm). The reduction of total PN concentration induced by both alcohols may obey to the same reasons argued above for PM reduction.

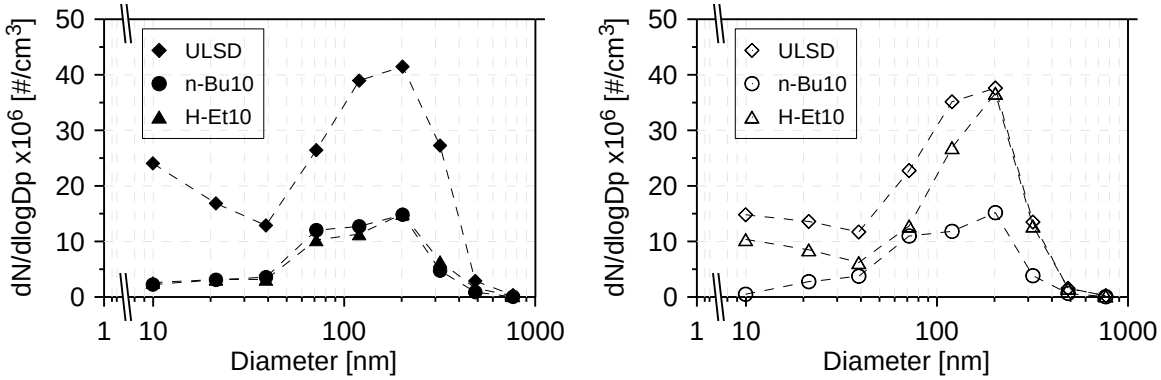

Fig. 9. Particle size distributions for mode M2 (left) and M4 (right)

A summary of the percentage of change of engine performance and emissions of alcohols fumigation with respect to ULSD is shown in

Table 5.

2.5 Conclusions

In this work an automotive diesel engine was modified with a built-in house multipoint port fumigation system to substitute 10% of diesel fuel in energy basis by hydrous ethanol and n-butanol in the intake manifold. Tests were carried out at three stationary engine operating modes in order to determine the impact of alcohols fumigation when fuel-air ratio and engine speed were varied. From this specific test conditions and engine technology it may be concluded that both alcohols increased CO and THC and simultaneously reduced NOx, PM and particulate number concentration compared to ULSD fuel, however the magnitude of this reduction was markedly affected by engine operating mode. Engine performance was deteriorated at low load due to poorer alcohols combustion, which showed the necessity of a minimum engine thermal load to start alcohols fumigation. Hydrous ethanol behaved different than n-butanol. At low engine speed and high fuel-air ratio, hydrous ethanol exhibited lower PM and higher specific NOx than n-butanol, however the contrary trend was observed at high engine speed and low fuel-air equivalence ratio. Finally, it is concluded that although both alcohols drastically reduced particulate number concentration,

these particulates did not show smaller nano-size geometrical diameter than ULSD fuel ones.

CHAPTER III: Impact of alcohol fumigation on the nanostructure and reactivity of diesel soot[2]

John R. Agudelo[1,], Andrés López[1], Marlon Cadrazco[1], Jesús Sánchez-Valdepeñas[2]*

[1]Departamento de Ingeniería Mecánica.
Universidad de Antioquia (UdeA). Calle 70 No. 7 52-21, Medellín, Colombia.

[2] Universidad de Castilla-La Mancha (Spain)

3.1 Abstract

A 2.5l turbocharged automotive diesel engine, modified with an intake multipoint port injection (IMPI) system to partially substitute ultra-low sulfur diesel (ULSD) fuel by hydrous ethanol (H-Et) and n-butanol (n-Bu), was used. Substitutions of diesel fuel in energy basis under two different stationary engine operating modes (43Nm and 95Nm at the same engine speed of 2410 min^{-1}) were successfully achieved. Particulate matter (PM) was collected through a stainless steel filter located 1.5m away from the exhaust system where the gas temperature was below 200ºC. In order to characterize its chemical composition and nanostructure characteristics, this PM was submitted to TGA and DRIFT for chemical composition, XRD and Raman spectroscopy for nanostructure and TEM and SEM for morphology. Results showed that, independently of the mode, soot produced with alcohol fumigation is more reactive to oxidation compared to ULSD, and follows the order H-Et > n-Bu > ULSD. This study also found that oxidation reactivity is affected by the chemical composition of the soot but not by its nanostructure. Soot nanostructure and morphology are not affected by engine load.

Keywords: fumigation, n-butanol, hydrous ethanol, diesel engine, oxidation reactivity

3.2 Introduction

Fuels derived from biomass such as biodiesel and alcohols are being used as partial surrogates of conventional diesel fuel. Alcohols become useful because they contain oxygen, which provides the potential to reduce particulate matter (PM) emissions [1]. Alcohol-diesel blends (mainly with ethanol or e-diesel) is the method most implemented in diesel engines, in spite of well-known associated issues: limited solubility [3], corrosion of the injection system due to water content [6], low lubricity [7], evaporation losses in fuel systems [9]. Alcohol fumigation is the addition of alcohol into the intake manifold and represents a viable alternative to avoid the problems of the direct blending. This technique,

[2] [2] This chapter has been submitted for publication at Combustion and Flame a journal from Elsevier

although requires an additional fuel tank and fuel injection system, enables to displace up to 50% of diesel energy demand in contrast with the limit of 25% for blends [3]. Many authors have shown that, independently of type of alcohol, fumigation i) reduces simultaneously particulate matter (in mass and number) and NOx emissions, ii) does not affect the geometrical mean diameter of the particulate and iii) increases the CO and THC emissions [10, 12-14, 18, 26-28, 30, 32-37, 52-56]. However, in author's knowledge there are no studies about how alcohol fumigation affects the oxidation reactivity, nanostructure and morphology of the particulate matter.

The soot nanostructure and its reactivity affect the performance and lifetime of diesel particulate filter (DPF), and its chemical composition provides valuable information of its potential hazards to human health. The understanding of these interactions allows that i) automotive industries can design properly DPF devices and ii) governments can promulgate more stringent environmental regulations, based on scientific evidence, to mitigate the impact of diesel exhaust particles on public health.

Studies about soot nanostructure have been carried out through different techniques that are listed in Lapuerta et al. [24]. The oxidation of the soot has been addressed with diverse approaches: i) the Arrhenius-type equation [57-66]; ii) a simplified rate expression for carbon oxidation which allows computing an apparent rate constant (lumped parameter) under isothermal oxidation conditions [67, 68]; iii) shrinking sphere model, where changes in the primary particle diameter are translated into mass loss [69, 70] and iv) direct comparison of burn-off curves from thermo-gravimetric analysis (TGA) [71-76] or temperature programmed oxidation (TPO) [77-79]. Combinations of these models also have been used. Kittelson and co-workers [80-83] used a high-temperature oxidation coupled to a tandem differential mobility analyzer (HTO-TDMA) to obtain kinetic parameters from the observed decreases in particle size using a modified form of the Arrhenius expression for the size decrease rate.

The initial fuel identity, as well as the engine speed and combustion temperature (fuel-air ratio), play major role in soot formation-growth-oxidation, affecting its chemical composition and nanostructure. For instance, oxygen and aromatics content in the fuel [67, 84] and its molecular structure [69, 85] has a great influence on soot reactivity and nanostructure. Engine operating conditions also affects the properties of the soot. Various studies [86-88] have shown that soot become more ordered as the in-cylinder temperature increases, according with the conceptual model of Marsh and Griffiths [89]. Recent works [24, 64, 83, 90] have shown that, in comparison with conventional diesel, oxygenated fuels generate soot with high graphitization degree and high oxidation reactivity. This fact shows that soot with high-disordered graphene layers is it not necessarily correlated with fast oxidation.

In this work, the chemical composition, nanostructure and morphology of the soot emitted by an automotive diesel engine modified with a multipoint intake n-butanol or hydrous ethanol fumigation system were investigated. TGA was used to study soot oxidation reactivity, active surface area and proximate analysis; main functional groups were identified by DRIFT spectroscopy. Soot nanostructure was determined through XRD and Raman spectroscopy. SEM was used to characterize the morphology of the agglomerates and finally, the mean geometric diameter and fractal dimension of primary particles were obtained from TEM micrographs.

3.3 Methodology

3.3.1 Engine test rig

Experiments were carried out in a 2.500 l, turbocharged, DI automotive diesel engine (Table 6) which was modified with a homemade intake multipoint port injection system (Fig. 10 and Fig. 11) to substitute 10% of diesel fuel in energy by hydrous ethanol (H-Et10) and n-Butanol (n-Bu10). The engine was coupled to a Schenck W230 eddy current dynamometer. The air consumption was measured with a Magnetrol TA2 hotwire sensor, and the diesel and alcohols fuel flows were measured with two separate Shimadzu electronic weight scales (±0.01 g). The instantaneous in-cylinder and injection pressures were recorded with Kistler 6056A piezoelectric pressure transducers coupled to Kistler 5011B charge amplifiers. The instantaneous piston position was measured with a Heidennhain ROD 426 angular encoder of 1024 pulses/rev. High speed data were acquired using the Labview™ software and a National Instruments™ data acquisition system (NI PCI 6024E and NI PCI MIO-16E-4). A zero-dimensional, one-zone thermodynamic combustion diagnosis model based on in-cylinder pressure signal was used here [38]. A total of 100 pressure curves were registered at each operation mode to ensure reliability in the combustion diagnosis results, obtaining a coefficient of variation (COV) of the indicated mean effective pressure lower than 5.2% for all tests performed. Total hydrocarbons (THC) emissions were registered with a ThermoFID 2000e flame ionization detector through a heated line (190 °C). Specific PM was obtained with a dilution rate of 10 through a Ricardo partial dilution tunnel. Whatman microfiber glass filters of 47 mm diameters were conditioned to 22 °C and 45% humidity for 48 h before and after PM collecting procedure. A Shimadzu high precision weight scale ($\pm 1 \times 10^{-5}$ g) was used to determine the collected mass of PM. The size and number of PM were acquired with a Dekati Electrical Low-Pressure Impactor (ELPI).

Table 6. Automotive diesel engine characteristics.

Reference	Isuzu 4JA1,
Type	4 in-line, 4-stroke, Turbocharged, DI, rotary pump
Swept volume [cm^3]	2499
Bore x stroke [mm]	93 x 92
Compression ratio	18.4
Rated power	59 kW at 4100 min^{-1}
Maximum torque	170 at 2300 min^{-1}

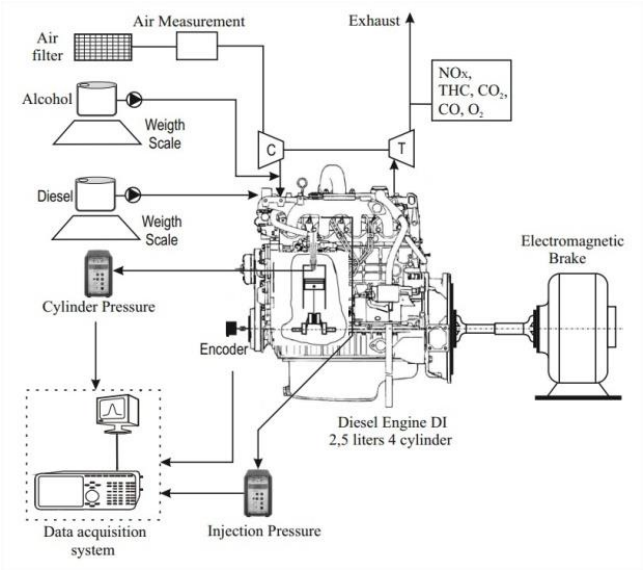

Fig. 10. Experimental setup

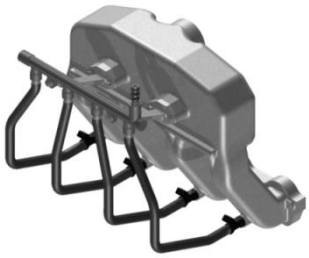

Fig. 11. Alcohol fumigation system

3.3.2 Electronic fumigation system

Both alcohols were injected at a pressure of 300 kPa. The needle lift of each injector was controlled with a homemade electronic control unit which was programmed in a *Freescale*™ microcontroller using *Labview*™ software. To ensure the synchronization of the alcohols injection, a proximate sensor was installed in the intake valve of cylinder #1. An engine speed sensor of 60 pulses per revolution of crankshaft was also implemented. Both sensors were connected to the microcontroller, which was programmed to configure and manage the alcohols injection process. The algorithm first configures the initial parameters for the correctly operation of the microcontroller; then it sets the injector opening time from the Labview-based software. Then it locates the top dead center (TDC) of the intake of cylinder #1 in order to synchronize the injection process of all alcohol injectors, which followed the order *2-3-4-1*, and finally it determines the needle opening time (ms) according to the set point established by the user (open loop).

3.3.3 Design of experiments

The engine was operated at 2410 min^{-1} and at two different loads, 43 Nm and 95 Nm (Table 7). The M2 operating mode (2410 min^{-1} and 95 Nm) was selected because it was the point of minimum air–fuel ratio and maximum smoke opacity according to the FTP75 homologation cycle, which was obtained by means of vehicle dynamics analysis. The mode M4 was selected in order to determine the impact of fuel-air equivalence ratio. Tests were carried out under carefully controlled operating conditions, so that the difference in performance and emissions were attributed only to fuels properties and configuration. To avoid dispersion of the results, the exhaust gas recirculation (EGR) valve was closed. A repeatability study of the test rig was carried out using a commercial diesel fuel. A set of 12 measurements were conducted during several days and different climate conditions. The uncertainty of the computed results was lower than its standard deviation. A 95% reliability level was reached by this repeatability study.

Table 7. *Operating conditions of selected modes with tested fuels.*

Name	% energy		Torque [Nm]	Speed [min^{-1}]	BMEP [bar]
	ULSD	n-Bu/H-Et			
M2 ULSD	100	0	95	2410	4.78
M2 H-Et10	90	10			
M2 n-Bu10					
M4 ULSD	100	0	43	2410	2.16
M4 H-Et10	90	10			
M4 n-Bu10					

3.3.4 Fuel properties

Hydrous ethanol (H-Et) was obtained from a local producer; chemical grade (99.9%) n-Butanol (n-Bu) was provided by a local distributor. Ultra-low sulfur diesel (ULSD) was supplied by the Colombian petroleum company (Ecopetrol) as a reference fuel (Table 8). After each alcohol was tested, fumigation system was drained prior to filling it with the next one. Then, the engine was operated for at least 15 min on the new fuel to purge any of the remaining non-test fuel from the engine fuelling system.

Table 8. Properties of ULSD), H-Et (94.16% w/w purity) and n-Bu (99.9 % w/w purity)

Fuel properties	**ULSD**	**Hydrous ethanol**	**n-Butanol [40]**
Chemical formula	$C_{14.7}H_{28.8}$	$C_{1.726}H_{5.452}O$	$C_4H_{10}O$
Density @ 15 ºC (kg/m^3)	856 [a]	809 [a]	810
Kinematic viscosity @ 40 ºC (cSt) [a]	3.625	1.454	2.500
Surface tension @ 25ºC (mN/m^{-1})	27.3 [41]	22.35 [42]	24.18 [43]
Cetane number	49	8	25
Lower heating value (kJ/kg) [a]	42,837	25,235	33,100
Molecular weight (kg/kmol)	205.2 [c]	42.2	74.0
Oxygen content (% weight)	0.0 [d]	37.9	21.6
C/H ratio	0.51[d]	0.32	0.40
Sulfur content (ppm)	<15 [d]	0	0
Water content (ppm)[a]	< 0.02	5.84	-
Latent heat of evaporation (kJ/kg)	265	948 [44]	585
Boiling point (°C)	202-362.5 [a]	77	118
Thermal conductivity (W/ m-K)[b]	-	0.165	0.153
Thermal diffusivity (Pa-s)[b]	-	0.123	0.091

[a] Measured, [b] Calculated, [c] Measured by vapor pressure osmometry (VPO), [d] Measured by elemental analysis (CHNOS).

3.3.5 Sampling procedure

Particulate matter was collected without dilution through a stainless steel 18/10 (18% Cr and 10% Ni) filter located 1.5m away from the engine in the exhaust system, where the gas temperature was below 200 ºC. A differential pressure sensor was installed to maintain the pressure drop at a maximum of 8 kPa. This value was selected because is a typical pressure drop value for the active regeneration of diesel particulate filters (DPF) [91]. For each test, measurements were carried out during 2 hours, being this time enough to collect the PM necessary for analysis.

3.3.6 Analytical techniques

3.3.6.1 Thermogravimetric analysis (TGA)

A Q500 thermogravimetric analyzer from TA Instruments was used to evaluate the oxidative reactivity, proximate analysis and active surface area (ASA) of all soot samples according to the procedure are listed in Table 9. The same procedure was followed for determining the proximate analysis and kinetics parameters. The devolatilization of the as-received PM sample was made through steps 1−3, i.e., subjecting the PM in a constant nitrogen atmosphere at 400 ºC and maintaining this temperature for long enough time to

ensure a complete removal of the water and volatile material. Previous works [60, 92] have established this temperature as the point at which most of the volatile organic material is gasified. After of this, the sample was cooled back down to 100 ºC, to take into account any possible soot oxidation at lower temperatures; then the surrounding atmosphere was switched to air (step 5). A heating ramp of 1 ºC/min from 100 ºC to 650 ºC (step 6) was used as recommended in [62]; this enables a complete soot oxidation. Once reached the final oxidation temperature (650 ºC) was kept during 30 min.

Oxidation reactivity of the soot was determined through the kinetic parameters (activation energy and frequency factor) of the Arrhenius-type equation, following the method proposed by Rodríguez-Fernández et al. [62]:

$$-\frac{dm}{dt} = k_c m^n p_{O_2}^r = A\ exp\left(\frac{-E_a}{RT}\right) m^n p_{O_2}^r \quad (1)$$

where m is the mass of the soot, t the time, k_c kinetic rate constant, p_{O_2} is the oxygen partial pressure (21 kPa), n and r are the reaction orders of sample and oxygen, respectively; A is the pre-exponential factor, E_a is the energy of activation, R is the universal gas constant () and T is the temperature. The reaction orders are simplified to unity [60, 62, 66].

$$ln\left(-\frac{dm}{mdt}\right) = ln\left(Ap_{O_2}\right) - \frac{E_a}{R}\frac{1}{T} \quad (2)$$

When logarithms are taken from eq. 1, results a line which is eq. 2. The slope of this trace (Arrhenius plot) is a function of the activation energy and the pre-exponential factor can be found through interception with the y axis. In the calculation of the kinetic parameters, the temperature range that leads to the most linearity (determined by R^2 coefficient) was used, corresponding to the soot weight loss of 10%−50% [66].

Active surface area was determined following the procedure listed in Table 4 as recommended by Al-Qurashi and Boehman [73]. Based on the amount of oxygen adsorbed on the soot, the ASA was calculated as follows [93]:

$$ASA = \frac{N_0 \sigma_0 N_A}{w_i} \quad (3)$$

where N_0 is the number of moles of chemisorbed oxygen, σ_0 is the area occupied by each oxygen atom (0.083 nm^2), N_A is the Avogadro´s number and w_i is the initial mass of soot.

Table 9.Summary of TGA procedures.

Step	Proximate analysis and oxidation	Active surface area
1	Start with high purity N_2 (100 mL/min)	
2	Heating to 400 °C and equilibrate	Ramp 10°C/min to 500°C
3	Isothermal for 60 min	Isothermal for 60 min
4	Equilibrate at 100 °C	Ramp 5°C/min to 200°C
5	Change atmosphere to air	Change to zero air (100 mL/min)
6	Heating ramp 1 °C/min to 650 °C	Isothermal for 10 hours
7	Isothermal for 30 min	Change to high purity N2 (100 mL/min)
8		Isothermal for 90 min

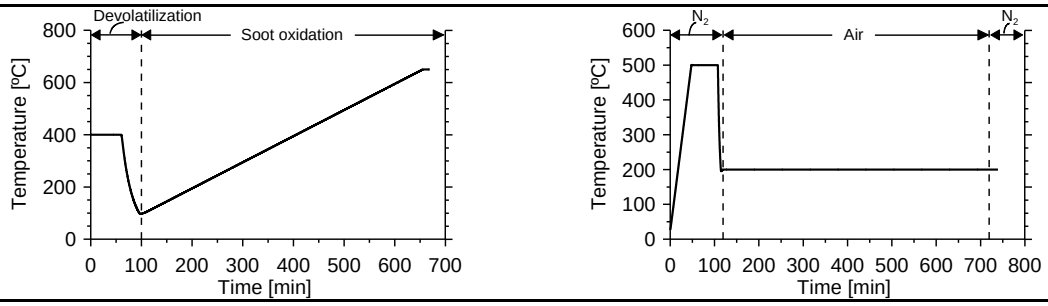

3.3.6.2 Diffuse Reflectance Infrared Fourier Transform spectroscopy (DRIFT)

A six mirror Harrick Scientific diffuse reflectance device model DRP-M-05 was coupled to a Shimadzu IR Prestige-21 FT-IR analyzer. Soot samples were located in the CHC-CHA-3 reaction chamber provided with a 3-windows dome, two of selenium zinc (ZnSe) and the third was made of quartz. CO2 was eliminated through a purge kit to avoid its interference in the spectroscopy analysis. Additionally a vacuum pump was connected to the main chamber to avoid air humidity effects. This technique was preferred over FT-IR spectroscopy to determine aromatics C-H, since PM is composed of large aromatic units with low hydrogen content at the periphery that cannot not be revealed by FT-IR through the C-H stretching mode [94].

3.3.6.3 X-Ray Diffraction spectroscopy (XRD)

XRD spectra were recorded in a Panalytical Xpert Pro MPD with a standby of 30kV to 10mA; the essay was run at 45kV to 40mA. A beam mask of 10 mm with a slit of 0.5 deg., with a copper radiation source of 1.54059 Å wave lengths was used. The start angle was 10° and the end angle was 80° with a step of 0.0263 and a time per step of 196.35 s which leads to a scan speed of 0.034105 (°/s). Curve fitting for the determination of lattice parameters were made through six pseudovoigt functions over the non-smoothed spectra with a fixed background. The background was fixed in the angle range of analysis (2θ = 10º

- 60º) by selecting a few points and fitting the adjacent two points with a third order spline function. Two pseudovoigt for the first peak (at 2θ = ~10º and ~24º) and other four functions for the second peak (at 2θ = ~38º, ~43.4, 43.56 and ~50º) were fitted (Fig. 12). The credibility of profile fitting was examined with residual error of fit (RMS) which was below 1.5% for all samples. La, Lc and d002 parameters were calculated based on the Scherrer equation and on the Bragg's law [95]. 2θ = ~19º band (and its reflection 2θ = ~38º) has been related to either amorphous characteristics of the sample, which can induce the buckling and exfoliation of the carbon layers [96] or to the presence of condensates in the VOF of PM samples [97]. There is a sharp peak at 2θ = 43.56º owing to the presence of iron in the soot as a consequence of the use of stainless steel filters [98].

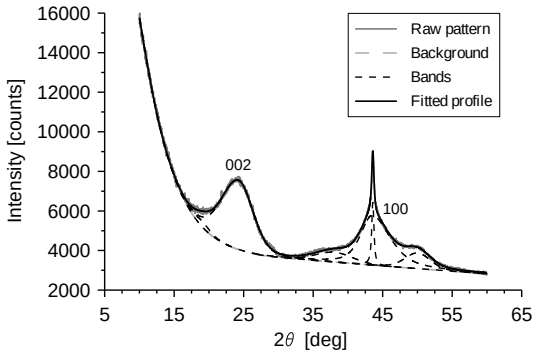

Fig. 12. Curve fit for the XRD spectrum of M4 ULSD.

3.3.6.4 Raman spectroscopy

Raman spectra of the soot samples were recorded with a LabRam HR Horiba microscope system using a 632.8 nm He/Ne laser excitation source. Spectra of the samples were in the range of 100–3600 cm-1 with a 50X magnification objective. In order to avoid altering or burning the sample, a 20 s exposition time and a source power of 0.17 mW were used [99]. Four curve-fitting method was employed for first-order Raman spectra as recommended by Sadezky et al. [100] and Seong and Boehman [76] for diesel carbonaceous material. Three Lorentzian functions for G band ~1580 cm^{-1}, D1 band ~1360 cm^{-1} and D4 band ~1180 cm^{-1} and one Gaussian function for D3 band ~1500 cm^{-1}) were used. However, no appreciable D2 band (around 1620 cm^{-1}) was exhibited by any sample. Four different spots were analyzed and averaged for each sample in order to improve the statistical significance.

3.3.6.5 Transmission Electron Microscopy (TEM)

Information of the primary particulate size of PM was obtained by TEM. A small amount of soot previously conditioned in a dichloromethane bath and cleaned with ethanol was deposited on a lacey carbon Formvar grid. Then it was placed in a JEOL JEM 1200EX microscope operated at a voltage range between 20 and 120 kV. Mean geometric particle

diameter was determined through a homemade software which takes a 100 nm scale as reference. For each fuel, the primary particle diameter was obtained as an average of 100 particulates of different sizes (10 particulates randomly selected of a micrograph times 10 different micrographs). Digital image processing of PM was implemented to calculate the fractal dimension (Df) of the agglomerates according to:

$$n = k_f \left(\frac{R_g}{d_p}\right)^{D_f} = \left(\frac{A_a}{A_p}\right)^{z} \quad (4)$$

where n is the number of primary particles per agglomerate, k_f is the prefactor, and R_g the radius of gyration of aggregates; A_a is the projected area of a particle agglomerate and A_p is the cross-section area of a primary particle and z is the overlapping factor. Moment of inertia, R_g, k_f and z were determined as a function of n by means of potential interpolations between the extreme cases (Df = 3 and Df = 1) [101]. Fractal dimension (D*f*) is a measure of the compactness of the primary particle clusters (agglomerate). Low D*f* implies more agglomerates with chain-like structure, while high D*f* indicates more compactly clustered primary particles (agglomerates forming a sphere has *Df* = 3 and an aligned chain of primary particles has *Df* = 1).

3.3.6.6 Scanning Electron Microscopy (SEM)

Morphology of the agglomerates was obtained through SEM micrographs. A small amount of PM was previously covered with a gold film, then it was placed in a JEOL JSM-6490 microscope operated at an accelerating voltage of 30 kV with a 40000X magnification.

3.4 Results and discussion

3.4.1 Composition evaluation

3.4.1.1 Volatile organic fraction (VOF) and active surface area (ASA)

Table 10. Emissions, VOF and ASA.shows that alcohol fumigation decreased specific PM emissions in comparison with ULSD, regardless the engine operating mode. This fact has commonly been explained as follows: i) the significant molecular oxygen content of both alcohols led to a higher PM oxidation rate in comparison to PM formation [49] and ii) as less mass of ULSD is injected, the C/H ratio of fuel-air mixture is smaller and additionally, less aromatics and sulfur components are available for PM formation. The higher emission of PM, obtained at mode M4, can be explained due to the lower in-cylinder temperature compared to mode M2.

.

Table 10. Emissions, VOF and ASA.

Mode	Fuel	In-cylinder Tmax [ºC]	PM [g/kWh]	THC [g/kWh]	VOF [%]	ASA [m2/g]
M2	ULSD	1583	0.470	0.326	0.743	0.80
	n-Bu10	1568	0.361	1.337	4.285	2.58
	H-Et10	1462	0.444	1.816	5.050	2.63
M4	ULSD	1329	1.265	1.364	8.347	2.40
	n-Bu10	1249	1.125	6.695	8.628	3.06
	H-Et10	1212	0.652	7.383	17.467	5.12

The VOF values obtained with alcohol fumigation are higher than those obtained with ULSD and are consistent with high THC emissions in alcohols. THC and their partial oxidation products are adsorbed as organic material onto the soot cores. Both alcohols emitted more THC than diesel fuel, however, the H-Et produced higher THC emissions than n-Bu. The combustion quenching (which causes an incomplete oxidation, specially at low load) due to the high heat of vaporization of alcohols and the alcohol reaching the oil layers in the piston rings have been the reasons to explain the THC increase [16, 83, 84]. VOF values follows the order H-Et > n-Bu > ULSD as does the soot reactivity (see Fig. 15). Although higher VOF of PM provides additional reactive hydrocarbons to oxidize catalytically in the DPF [28], the VOF content was not take into account for explain soot reactivity since the VOF does not take part in the soot oxidation test in this study (see procedure in Table 9.Summary of TGA procedures.). Table 10 also shows the results of ASA, which is a parameter associated with active sites in PM surface [29, 73]. This values exhibited the same trend than those obtained in VOF and may not to be a coincidence, because there is a high probability that the oxygen atoms have an affinity for those areas that were occupied by the organic compounds before the devolatilization.

3.4.1.2 Functional Groups

The spectra were normalized using the most prominent peak of the aliphatic group according to the method proposed by Santamaría et al. [85]. The presence of aliphatic structures is represented by three characteristic sharp peaks at 2975 (Methyl asymmetric C-H stretch), 2925 (Methylene asymmetric C-H stretch) and 2850 cm^{-1} (Methylene symmetric C-H stretch). Figure 13 does not show the fingerprint region (1250 – 1850 cm-1) because there was no significant differences among samples.

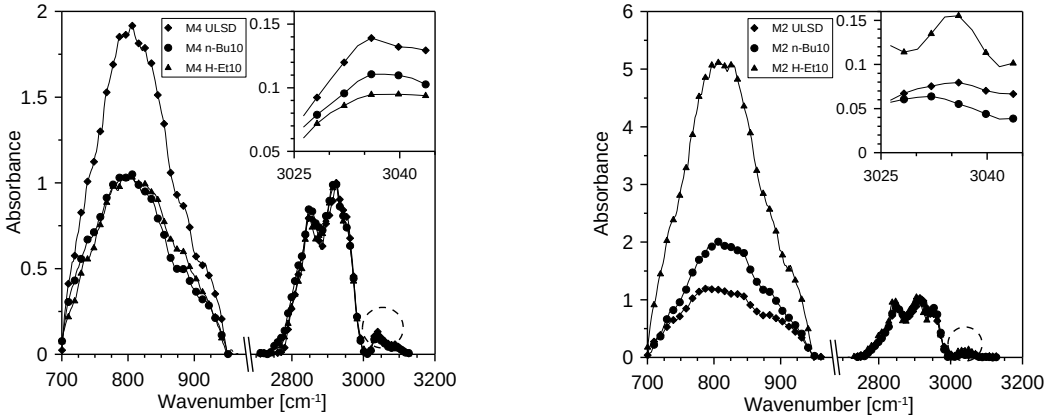

Fig. 13. C=C–H out-of-plane aromatics and aliphatics groups by DRIFT spectroscopy.

The region between 700 cm^{-1} and 900 corresponds to C=C–H out-of-plane bending (wagging) vibrations of isolated hydrogen (880–870 cm^{-1}), two- (830–800 cm^{-1}), three- (800–770 cm^{-1}) and four-adjacent hydrogen atoms (760–735 cm^{-1}) of condensed aromatic systems [85]. This bands are much stronger than the aromatic C-H stretching vibrations (3100–2800 cm^{-1} region) and can be used to quantify the aromatic hydrogen when: (i) the aromatic C-H stretching signal is too low to be detected or (ii) when the presence of water makes difficult a right evaluation of aromatic C-H stretching peak height due to the distorted baseline for effect of O-H stretching peak at around 3200 cm^{-1} [86]. All spectra exhibited significant changes at this region, particularly at 805 cm^{-1} which means that there are a high concentration of two adjacent hydrogen atoms in poliaromatic structures. The study conducted by Russo and collaborators [86] concluded that the quantification of aromatic hydrogen in terms of solo, duo and trio/quatro allows to assess the lower abundance of solo hydrogen in favor of duo and trio/quatro hydrogen probably related to the issue of edge topology of aromatic clusters. Based on this, the high intensity of the peak at 805 cm^{-1} could be related with the presence of armchair-type edge defects, which implies more active sites for oxygen attack.

3.4.1-3 Soot oxidation reactivity

Typical temperatures of the oxidation process over TGA profiles of the M2-ULSD soot sample are shown in Fig. 14 (right). These characteristic temperatures according to

Rodríguez-Fernandez et al. [40] are: the starting oxidation temperature (SOT) and the maximum mass loss rate temperature ($MLRT_{max}$). Low SOT and $MLRT_{max}$ temperatures imply earlier and faster oxidation reactivity, respectively, which means lower requeriments of energy. Regardless the mode, soot from both hydrous ethanol and n-butanol have lower $MLRT_{max}$ in comparison with soot coming from ULSD (see Fig. 14), meaning that a high fraction of soot produced under alcohol fumigation is oxidized before than soot emitted by reference fuel. This fact has a positive effect on the global fuel penalty reducing the fuel injection during active regeneration on DPF devices. The oxidative behavior also can be addressed by the kinetic constant. Again, is clearly shown in Fig. 15 that, independently of the mode, soot from alcohol fumigation is oxidized faster (high k_c) than ULSD soot, having the hydrous ethanol the larger values.

2.

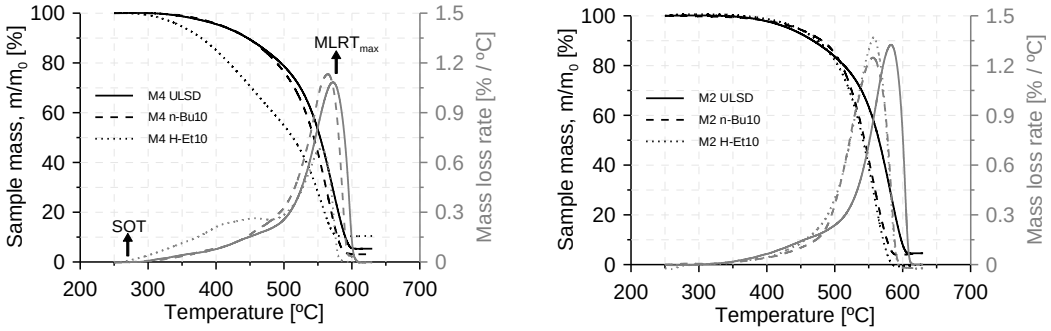

Fig. 14. Mass loss and mass loss rate for modes M2 (left) and M4 (right).

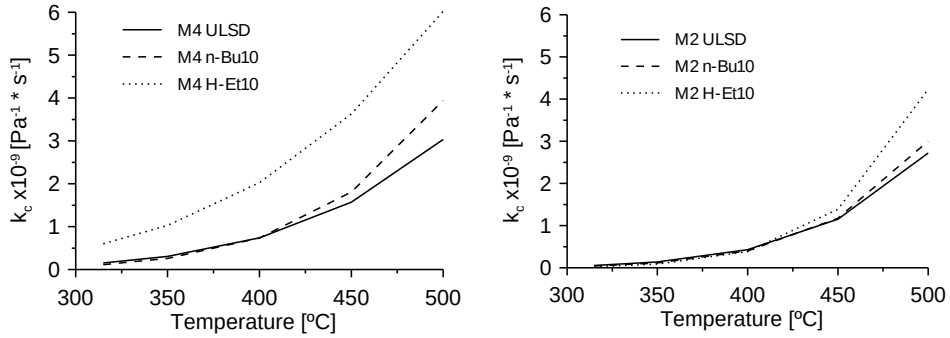

Fig. 15. Kinetic constant as a function of temperature.

Differences in oxidation reactivity of alcohol-derived soot samples, when compared to ULSD, could be explained by the effect of the active surface area (Fig. 16). The relationship between ASA and oxidation has also been previously presented [29, 36, 50, 87]. ASA values are plotted against $1/t_{50\%}$ in Fig. 16. The variable $1/t_{50\%}$ is the inverse of the time (computed from the start of the change to oxidative atmosphere in TGA program, step 5) needed for reaching the 50% of the mass loss. Although the relationship is not linear (R^2 = 0.95), ASA exhibited a good correlation with oxidation reactivity. In particular, regardless the mode, soot from hydrous ethanol has the highest ASA, resulting in faster oxidation

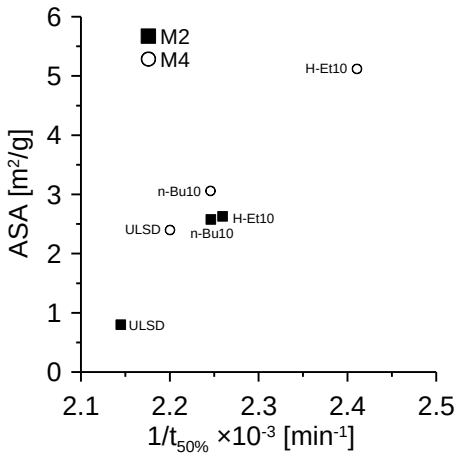

Fig. 16. ASA against oxidation reactivity.

3.4.2 Soot morphology

Fig. 17 and Fig. 18 display that, despite the engine load and fuel operation, the mean diameter of both agglomerates and primary particles remain constant. Similarly, Fig. 19 shows that another morphological parameter as *Df* exhibited no significant differences when alcohol fumigation was applied. Yao et al. [88] and Zhang et al. [89] reported that although alcohol fumigation reduces the number of total particles, does not significantly change the diameter of the particles.

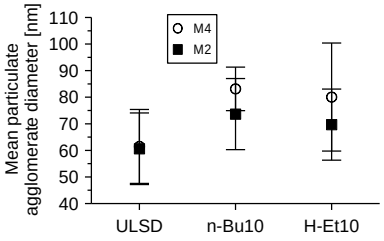

Fig. 17. Diameter of agglomerates.

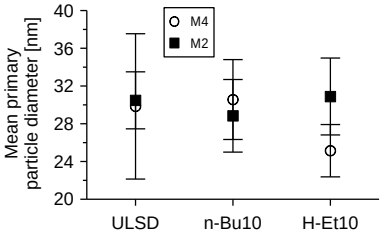

Fig. 18. Primary particle diameter.

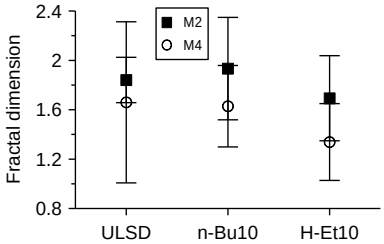

Fig. 19. Fractal dimension of the aggregates

SEM and TEM images of the PM samples are shown in Fig. 20 and Fig. 21 respectively. Regardless the mode and fuel, PM exhibited the classic sphere chain-like agglomerates, i.e., there is no difference in micro-scale morphology among the PM produced by ULSD and alcohol fumigation. The morphology of nano-sized particles also presents negligible differences when comparing among fuels and between modes.

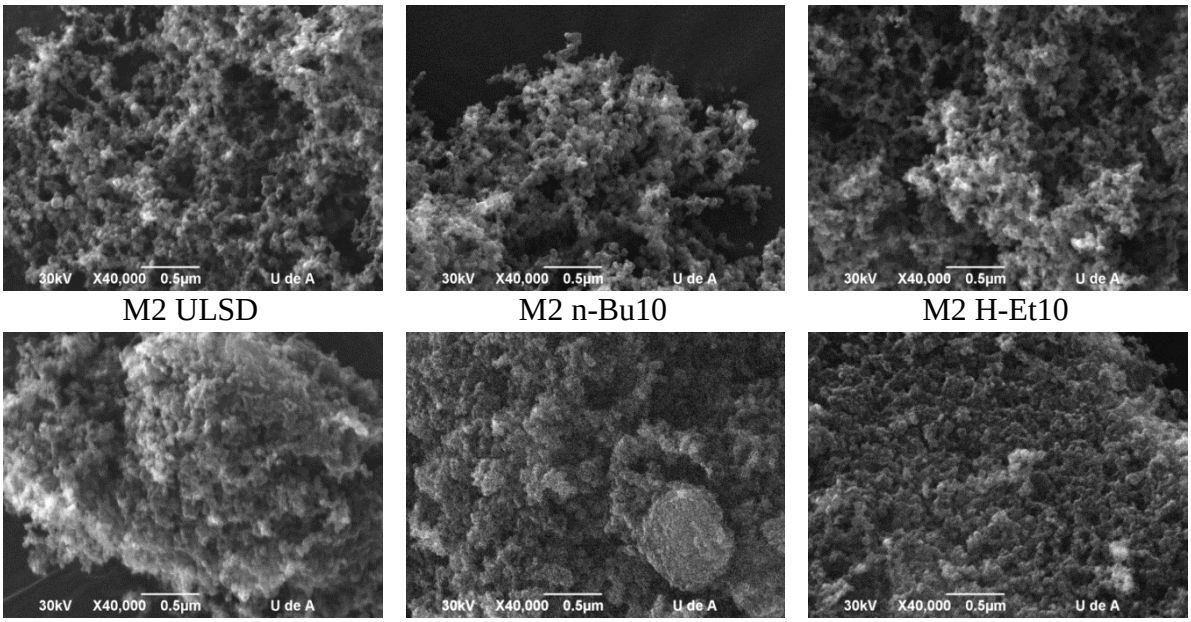

M2 ULSD M2 n-Bu10 M2 H-Et10

M4 ULSD M4 n-Bu10 M4 H-Et10

Fig. 20. SEM micrographs

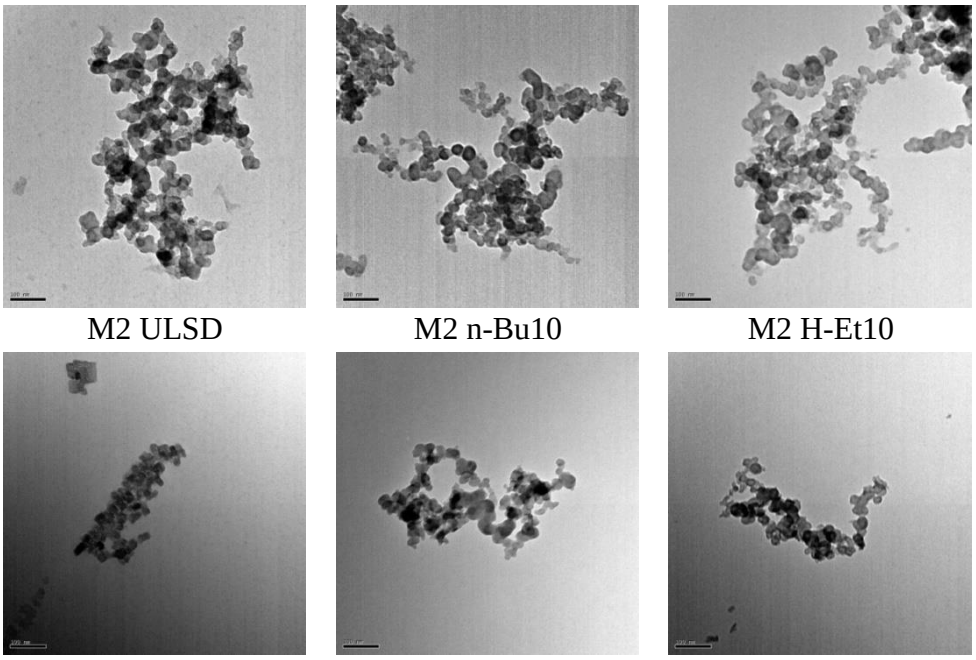

M2 ULSD M2 n-Bu10 M2 H-Et10

M4 ULSD M4 n-Bu10 M4 H-Et10

Fig. 21. TEM images of primary particles aggregates

3.4.3 Nanostructural analysis (XRD and Raman spectroscopy)

Interplanar layer spacing (d_{002}), L_a and L_c dimensions are shown in Fig. 22 and Fig. 23 respectively. The alcohol fumigation produced no significant differences in d002 values

(less than 0.05 angstrom) as well as in crystallite parameters Lc and La in comparison with ULSD. These differences are still negligible between modes M2 and M4.

This behavior was also noted in the information of graphite-like structure determined by Raman spectroscopy. The degree of order (I_{D1}/I_G ratio) as well as the information related with the presence of interstitials defects (I_{D3}/I_G ratio) and polyene-like structures (I_{D4}/I_G ratio) in graphene planes are shown in Fig. 24. One more time it can be noticed that the fumigation of hydrous ethanol and n-butanol did not affect the soot nanostructure in comparison with ULSD. Likewise, the effect of the engine torque at constant engine speed is not evident. Yehliu et al. [45] showed that equivalence ratio (at engine speed = constant) hardly affects the soot nanostructure; in contrast, the engine speed at constant torque yielded a pronounced impact.

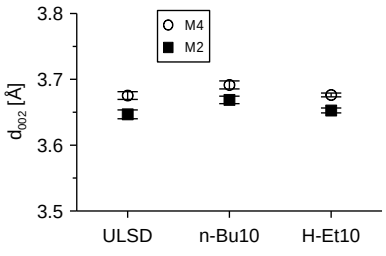

Fig. 22. Interplanar distance between carbon layers (d002).

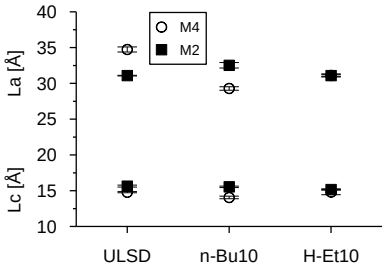

Fig. 23. Stacking thickness (Lc) and length of the fringes (La) of soot.

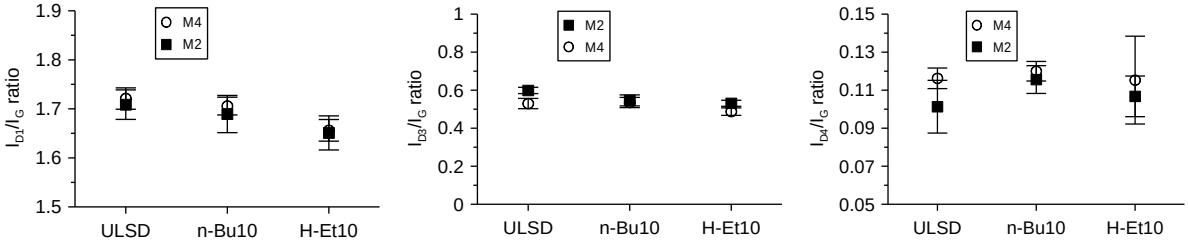

Fig. 24. Raman peaks intensity ratios of soot samples

3.5 Conclusions

Under this test conditions and engine configuration, it can be concluded that the use of alcohol fumigation affects the chemical composition and therefore the oxidation reactivity of diesel particulate matter which is a relevant finding for the proper design of after-treatment systems such as diesel particulate filters (DPF) and provides valuable information about potential hazards to human health. The following conclusions can be drawn from the experimental work conducted in this investigation:

- Independently of the mode, soot produced with fumigation of alcohols is more reactive to oxidation compared to ULSD, and follows the order H-Et > n-Bu > ULSD.

- Oxidation reactivity is affected by the chemical composition (i.e., active surface area) of the soot but not by its nanostructure, and follows the order H-Et > n-Bu > ULSD.

- Soot nanostructure and morphology are not affected by alcohol fumigation neither by engine torque (at constant engine speed).

CHAPTER IV: Genotoxicity of Particulate Matter

4.1 STATE OF THE ART

4.1.1 Why to study the biological toxicity of the PM?

In 2012, the International Agency for Research on Cancer (IARC) classified diesel engine exhaust as Group 1 (carcinogenic to humans) in especial PM [46], based on evidence that exposure of diesel exhaust had an increased risk for lung cancer. This PM is characterized by a carbonaceous core (soot) and it have sulfur oxides, nitrogen oxides and other compounds such as polycyclic aromatic hydrocarbons (PAHs) onto the surface [90]. PAHs are agents that are formed by incomplete combustion of organic matter and cause significant damage to DNA, specifically the formation of adducts, which generate a genotoxic damage [42, 47].

4.1.2 Effect of the alcohol fumigation on the PM toxicity

An assessment of the biological activity of the exhaust particulate and its soluble organic extract was made by Houser et al [109]. This study indicates that methanol fumigation can increase the biological activity, as measured by the Ames *Salmonella typhimurium* and the *Bacillus subtilis* tests, of both the raw particulate matter and its soluble organic fraction. Broukhiyan and Lestz [110] evaluated the effect of ethanol fumigation on the emissions of a light-duty automotive diesel engine. For all conditions tested, ethanol fumigation not only reduced NOx and PM concentrations, but also increased the biological activity of the particulate (Ames *Salmonella typhimurium* assay). Heisey and Lestz [111] fumigated aqueous alcohol on a single-cylinder DI engine to evaluate the same parameters of previous work [109, 110]; they found that aqueous ethanol fumigation increases the biological activity measured by the Ames test, of the raw particulate and its soluble organic extract.

Surawski et al [29] studied the volatility and toxicity of PM produced by a CI engine pre-Euro I, to assess the potential health impacts generated by the use fumigation of ethanol. A profluorescent nitroxide probe, BPEAnit, was used to investigate the potential toxicity of particles. They reported an increase in the volatility and toxicity of soot, because the fumigation coated the particles with organic material.

4.2 METHODOLOGY

4.2.1 SOF extraction

Soluble organic fraction (SOF) from the PM collected (see section 2.2.4.) was obtained through the method proposed by Singh et al. [112]. 50 mg of the PM was mixed with 100 ml of dichloromethane (DCM) and the mixture was vortexed 2–3 min. The tubes, with the PM-DCM mixture, were placed in a sonicating bath for about 1 hour and centrifuged at approximately 2,000 rpm for 10 min, and the solvent was transferred to another glass tube. This extraction was repeated two more times. Then, each sample was filtered through 0.22 µm nylon membranes to obtain a SOF-DCM mixture. Finally, the organic solvent (DCM)

was rota-evaporated to a volume of 1 ml and concentrated under a stream of N_2. The SOF was diluted in 10% dimethyl sulfoxide (DMSO) for genotoxic analysis and, since it was not possible to determine the weight of SOF, the concentrations were expressed as the equivalent amount (µg-eq) of particulate matter [113].

4.2.2 Cell viability

To evaluate the effect of SOF on the DNA, human lymphocytes from heparinized blood (10 ml) were used. These were obtained from a 25-aged healthy volunteer with habits that do not imply a bias in research (e.g., no smoker). The lymphocyte separation was performed using the Ficoll gradient method [114]. In the cell suspension, cell viability was determined using trypan blue in a Neubauer chamber. The cell viability was calculated as follows:

$$\%V = 100 \times \frac{live\ cells}{total\ cells} \tag{5}$$

Only when the cell viability was greater than 95%, the lymphocytes were exposed to SOF [115]. Cell cultures, each one with 100,000, were subjected for 1 h to different concentrations of SOF, and then assessing the cell viability. Since the genotoxicity is associated to low or null cytotoxic effects [116], those post-treatment concentrations which led a viability greater than 75% ± 5 were chosen for further analysis.

4.2.3 Genotoxic potential assessment

100,000 cells approx. were treated for one hour with seven different concentrations (500, 250, 125, 63, 31, 16 and 8 µg-eq) of SOF. For this study, phosphate-buffered saline (PBS) was used as negative control, hydrogen peroxide (H2O2 100 µM) as a positive control [117] and 1% DMSO as solvent control. Then, alkaline comet assay [118] with modifications for including GelBond films [119] was performed. The electrophoresis was run at 25 mV and 300 mA (Power Pac 3000 BioRad) for 30 minutes in dark room at 4 °C. The Gelbond films were washed with neutralizing solution (0.4M Tris-HCl pH 7.5) and stained with 2 µl/ml of ethidium bromide.

Counting of the cells was performed in a Boeco fluorescence microscope with green filter and a magnification of 20x; the comet tails were measured through an ocular rule, adapted to the microscope. 100 random cells were analyzed per assay and 3 assays per dose. Damage in the DNA was determined using, as a reference, the mean of the tail length of the negative control (X±DS+1), i.e., 7+2+1=10 µm. The percentage of damaged cells (%DC), was calculated as:

$$\%DC = 100 \times \frac{cell\ with\ any\ damage}{total\ cells} \tag{6}$$

The damage levels were classified into five arbitrary categories according to the length of the comet tail: 0) null (<11 µm), i) low (11-34 µm), ii) medium (35-58 µm), iii) high (59-82 µm) and iv) total (>83 µm) damage. Therefore, the Weighted Damage Index (WDI) can be defined as [120]:

$$WDI = n_1 + 2n_2 + 3n_3 + 4n_4 \quad (7)$$

Where, n_1, number of cells with level 1 of damage; n_2, number of cells with level 2 of damage; n_3, number of cells with level 3 of damage; n_4, number of cells with level 4 of damage.

4.2.4 Statistical analysis

Since the coefficient of variation of the data was <10%, the results were homogenized and presented as the mean (± SD) of the comet tail length. The data distribution was determined by kurtosis and symmetry. The differences in the results was evaluated by the Kruskal-Wallis test, considering a significant difference of $p < 0.05$.

4.3 RESULTS AND DISCUSSION

Cell viability after 1 hour of treatment was >70% for all concentrations, thus it is inferred that genotoxic activity can be attributed to the SOF but no to external cytotoxic effects. All concentrations were significantly genotoxic ($p < 0.05$) compared to negative control. Regarding to WDI or magnification of the cell damage, it is statistical significant for all doses ($p<0.001$) and increases about 2 to 700 times the negative and solvent control values. Alcohol fumigation led more genotoxic activity than ULSD, and follows the order H-Et10 > n-Bu10 > ULSD, independently of the mode and concentration. However, as the concentration increases, the difference between alcohol fumigation and ULSD decreases.

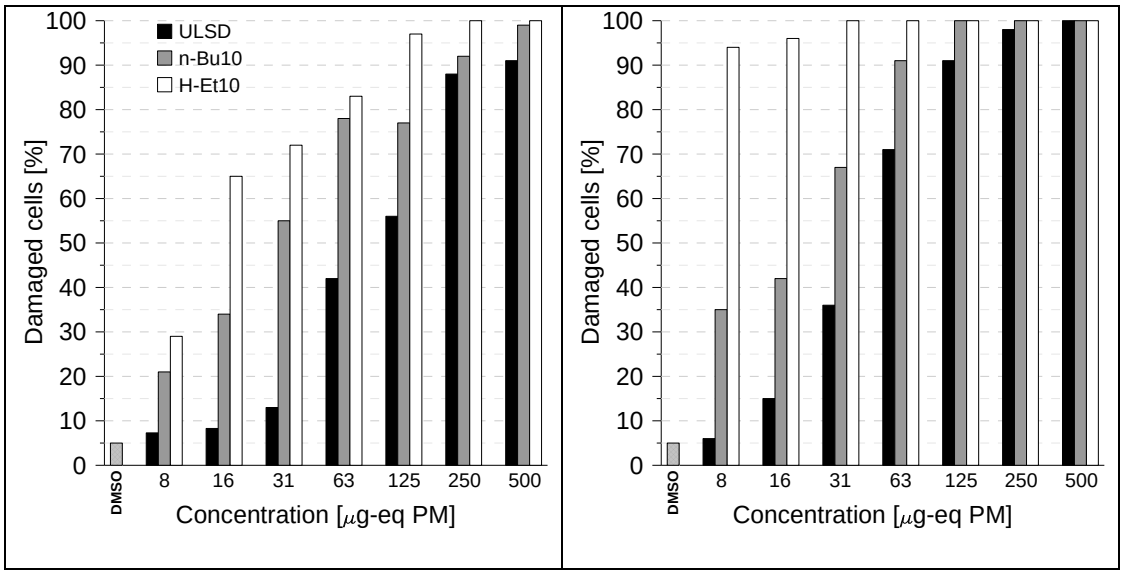

Fig. 25. Percentage of the damaged cells in modes M2 (left) and M4 (right).

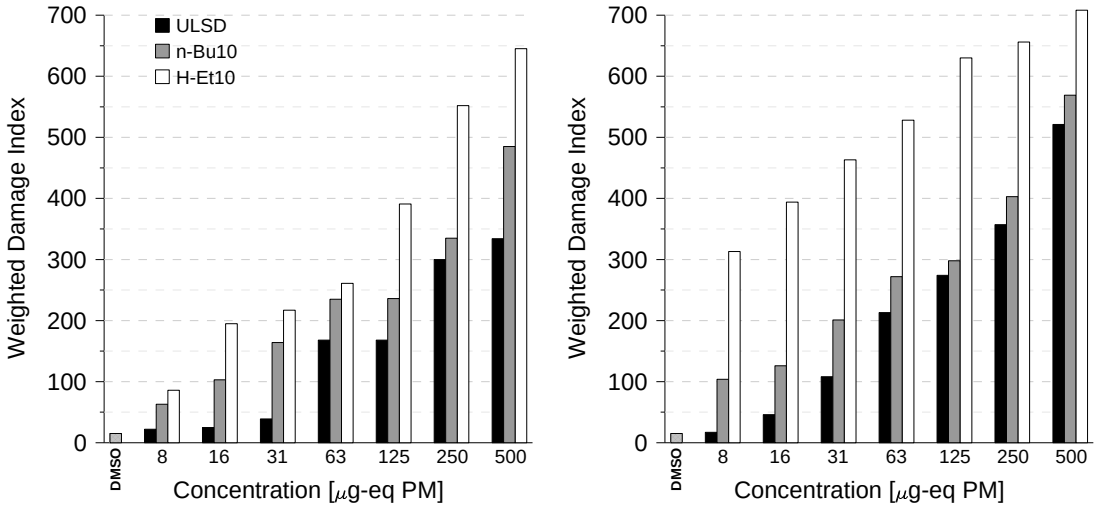

*Fig. 26***.** Magnification of the damage in modes M2 (left) and M4 (right).

The results showed in Chapter 3 demonstrate that PM from of alcohol fumigation is chemically different from the ULSD, therefore it was also expected that the biological response was different. Alcohol fumigation has proven to increase the aldehyde emissions [19, 21] which are compounds that increase the genotoxic biomarkers both in vivo and in vitro. Although this study does not determine how much aldehydes neither what species were produced, it is likely that PM from alcohol fumigation has aldehydes as a part of the SOF (or VOF), leading a more genotoxic activity compared to ULSD.

CHAPTER V: Conclusions and recommendations

5.1 Conclusions

In this work an automotive diesel engine was modified with a built-in house multipoint port fumigation system to substitute 10% of diesel fuel in energy basis by hydrous ethanol and n-butanol in the intake manifold. Tests were carried out at three stationary engine operating modes in order to determine the impact of alcohols fumigation when fuel-air ratio and engine speed were varied. From this specific test conditions and engine technology it may be concluded that both alcohols increased CO and THC and simultaneously reduced NOx, sPM and particulate number concentration compared to ULSD fuel, however the magnitude of this reduction was markedly affected by engine operating mode. Engine performance was deteriorated at low load due to poorer alcohols combustion, which showed the necessity of a minimum engine thermal load to start alcohols fumigation. Hydrous ethanol behaved different than n-butanol. At low engine speed and high fuel-air ratio, hydrous ethanol exhibited lower sPM and higher specific NOx than n-butanol, however the contrary trend was observed at high engine speed and low fuel-air equivalence ratio. Finally, it is concluded that although both alcohols drastically reduced particulate number concentration, these particulates did not show smaller nano-size geometrical diameter than ULSD fuel ones.

Under this test conditions and engine configuration, it can be concluded that the use of alcohol fumigation affects the chemical composition and therefore the oxidation reactivity of diesel particulate matter which is a relevant finding for the proper design of after-treatment systems such as diesel particulate filters (DPF) and provides valuable information about potential hazards to human health. The following conclusions can be drawn from the experimental work conducted in this investigation:

- Independently of the mode, soot produced with fumigation of alcohols is more reactive to oxidation compared to ULSD, and follows the order H-Et > n-Bu > ULSD.

- Oxidation reactivity is affected by the chemical composition (i.e., active surface area) of the soot but not by its nanostructure, and follows the order H-Et > n-Bu > ULSD.

- Soot nanostructure and morphology are not affected by alcohol fumigation neither by engine torque (at constant engine speed).

The biological analysis can be concluded that fumigation of hydrated ethanol and n-butanol substituting 10% diesel fuel, generates a soluble fraction in the particulate material having greater genotoxic effect that the diesel fuel reference, independent of the mode of operation motor (low and high load)

5.2 Recommendations

- To evaluate the effect of alcohol fumigation under transient modes
- To implement control strategies ensuring that the fumigation system can be used in vehicles
- To compare the effect of alcohol fumigation using different injection pumps
- To assess the mutagenic effect of particulate matter SOF
- To evaluate the biological activity effect of in vitro of the particulate material obtained alcohol fumigation
- To perform durability tests in order to evaluate the reliability of alcohols fumigation technique
- To continue researching in low temperature combustion concepts (RCCI: reactivity controlled compression ignition) with hydrous ethanol and n-butanol

REFERENCES

1. Hansen A, Zhang Q,Lyne P. Ethanol–diesel fuel blends – a review. Bioresource Technology 2005;96:277-285.
2. Can Ö, Çelikten İ,Usta N. Effects of ethanol addition on performance and emissions of a turbocharged indirect injection Diesel engine running at different injection pressures. Energy Conversion and Management 2004;45:2429-2440.
3. Ecklund E, Bechtold R, Timbario T,McCallum P. State-of-the-art report on the use of alcohols in diesel engines SAE Technical Paper 840118
4. Yilmaz N,Sanchez TM. Analysis of operating a diesel engine on biodiesel-ethanol and biodiesel-methanol blends. Energy 2012;46:126-129.
5. Lapuerta M, Armas O,García-Contreras R. Stability of diesel–bioethanol blends for use in diesel engines. Fuel 2007;86:1351-1357.
6. Agarwal AK. Biofuels (alcohols and biodiesel) applications as fuels for internal combustion engines. Progress in Energy and Combustion Science 2007;33:233-271.
7. Lapuerta M, García-Contreras R,Agudelo JR. Lubricity of ethanol-biodiesel-diesel fuel blends. Energy & Fuels 2009;24:1374-1379.
8. Li D-g, Zhen H, Lŭ X, Wu-gao Z,Jian-guang Y. Physico-chemical properties of ethanol–diesel blend fuel and its effect on performance and emissions of diesel engines. Renewable Energy 2005;30:967-976.
9. Lapuerta M, Hernández JP,Agudelo JR. An equation for the estimation of alcohol-air diffusion coefficients for modelling evaporation losses in fuel systems. Applied Thermal Engineering 2014;73:537-546.
10. Abu-Qudais M, Haddad O,Qudaisat M. The effect of alcohol fumigation on diesel engine performance and emissions. Energy Conversion and Management 2000;41:389-399.
11. Zhang ZH, Tsang KS, Cheung CS, Chan TL,Yao CD. Effect of fumigation methanol and ethanol on the gaseous and particulate emissions of a direct-injection diesel engine. Atmospheric Environment 2011;45:2001-2008.
12. Heisey J,Lestz S. Aqueous alcohol fumigation of a single-cylinder DI diesel engine. SAE Technical Paper 811208
13. Baranescu R. Fumigation of alcohols in a multicylinder diesel engine - Evaluation of potential. SAE Technical Paper 860308
14. Hayes T, Savage L, White R,Sorenson S. The effect of fumigation of different ethanol proofs on a turbocharged diesel engine. SAE Technical Paper 880497
15. Imran A, Varman M, Masjuki HH,Kalam MA. Review on alcohol fumigation on diesel engine: A viable alternative dual fuel technology for satisfactory engine performance and reduction of environment concerning emission. Renewable and Sustainable Energy Reviews 2013;26:739-751.
16. Tsang KS, Zhang ZH, Cheung CS,Chan TL. Reducing emissions of a diesel engine using fumigation ethanol and a diesel oxidation catalyst. Energy & Fuels 2010;24:6156-6165.
17. Havemann HA, Rao M, Nalaragan A,Narasimban TL. Alcohol in diesel engines. Automobile Engineer 1954;44:256-262.
18. Broukhiyan E,Lestz S. Ethanol fumigation of a light duty automotive diesel engine. SAE Technical Paper 811209

19. Van Gerpen JH,Van Meter D, *Emission control in diesel engines by alcohol fumigation*1990, Iowa: Midwest Transportation Center.
20. Kumar P, *Use of ethanol in CI engine*, 2006, Delhi University.
21. Zhang ZH, Cheung CS, Chan TL,Yao CD. Experimental investigation of regulated and unregulated emissions from a diesel engine fueled with Euro V diesel fuel and fumigation methanol. Atmospheric Environment 2010;44:1054-1061.
22. Cheng CH, Cheung CS, Chan TL, Lee SC, Yao CD,Tsang KS. Comparison of emissions of a direct injection diesel engine operating on biodiesel with emulsified and fumigated methanol. Fuel 2008;87:1870-1879.
23. Cheng CH, Cheung CS, Chan TL, Lee SC,Yao CD. Experimental investigation on the performance, gaseous and particulate emissions of a methanol fumigated diesel engine. Science of The Total Environment 2008;389:115-124.
24. Lapuerta M, Oliva F, Agudelo JR,Boehman AL. Effect of fuel on the soot nanostructure and consequences on loading and regeneration of diesel particulate filters. Combustion and Flame 2012;159:844-853.
25. Goering CE,Wood DR. Over fuelling a diesel engine with carbureted ethanol. Transactions of the ASAE 1982;25:576-580.
26. Ajav EA, Singh B,Bhattacharya TK. Performance of a stationary diesel engine using vapourized ethanol as supplementary fuel. Biomass and Bioenergy 1998;15:493-502.
27. Lu X, Ma J, Ji L,Huang Z. Simultaneous reduction of NOx emission and smoke opacity of biodiesel-fueled engines by port injection of ethanol. Fuel 2008;87:1289-1296.
28. Rodríguez-Fernández J, Tsolakis A, Theinnoi K, Snowball J,al. e. Engine performance and emissions from dual fuelled engine with in-cylinder injected diesel fuels and in-port ìnjected bioethanol. SAE Technical Paper 2009-01-1853
29. Surawski NC, Miljevic B, Roberts BA, Modini RL, Situ R, Brown RJ, et al. Particle Emissions, Volatility, and Toxicity from an Ethanol Fumigated Compression Ignition Engine. Environmental Science & Technology 2009;44:229-235.
30. Surawski NC, Ristovski ZD, Brown RJ,Situ R. Gaseous and particle emissions from an ethanol fumigated compression ignition engine. Energy Conversion and Management 2012;54:145-151.
31. Song R, Liu J, Wang L,Liu S. Performance and Emissions of a Diesel Engine Fuelled with Methanol. Energy & Fuels 2008;22:3883-3888.
32. Zhang ZH, Cheung CS,Yao CD. Influence of fumigation methanol on the combustion and particulate emissions of a diesel engine. Fuel 2013;111:442-448.
33. Michikawauchi R, Tanno, S., Ito, Y., and Kanda, M. Combustion improvement of diesel engine by alcohol addition - Investigation of Port Injection Method and Blended Fuel Method. SAE Int. J. Fuels Lubr. 2011;4:48-57.
34. Soloiu V, Duggan M, Harp S, Vlcek B,Williams D. PFI (port fuel injection) of n-butanol and direct injection of biodiesel to attain LTC (low-temperature combustion) for low-emissions idling in a compression engine. Energy 2013;52:143-154.
35. Chen Z, Liu J, Wu Z,Lee C. Effects of port fuel injection (PFI) of n-butanol and EGR on combustion and emissions of a direct injection diesel engine. Energy Conversion and Management 2013;76:725-731.

36. Zhu Y, Chen Z,Liu J. Emission, efficiency, and influence in a diesel n-butanol dual-injection engine. Energy Conversion and Management 2014;87:385-391.
37. Liu H, Wang X, Zheng Z, Gu J, Wang H,Yao M. Experimental and simulation investigation of the combustion characteristics and emissions using n-butanol/biodiesel dual-fuel injection on a diesel engine. Energy 2014;74:741-752.
38. Lapuerta M, Armas O,Hernández JJ. Diagnosis of DI Diesel combustion from in-cylinder pressure signal by estimation of mean thermodynamic properties of the gas. Applied Thermal Engineering 1999;19:513-529.
39. Benjumea P, Agudelo JR,Agudelo AsF. Effect of the Degree of Unsaturation of Biodiesel Fuels on Engine Performance, Combustion Characteristics, and Emissions. Energy & Fuels 2010;25:77-85.
40. Giakoumis EG, Rakopoulos CD, Dimaratos AM,Rakopoulos DC. Exhaust emissions with ethanol or n-butanol diesel fuel blends during transient operation: A review. Renewable and Sustainable Energy Reviews 2013;17:170-190.
41. Moser BR,Vaughn SF. Evaluation of alkyl esters from Camelina sativa oil as biodiesel and as blend components in ultra low-sulfur diesel fuel. Bioresource Technology 2010;101:646-653.
42. Vazquez G, Alvarez E,Navaza JM. Surface Tension of Alcohol Water + Water from 20 to 50 .degree.C. Journal of Chemical & Engineering Data 1995;40:611-614.
43. Benson GC,Lam VT. Surface tensions of binary liquid systems. II. Mixtures of alcohols. Journal of Colloid and Interface Science 1972;38:294-301.
44. Stein F, *The integral isobaric heat of vaporization of mixtures*, in *Industry program of the college of engineering*1960, The University of Michigan: Michigan.
45. Zhang Y,Boehman AL. Oxidation of 1-butanol and a mixture of n-heptane/1-butanol in a motored engine. Combustion and Flame 2010;157:1816-1824.
46. Dagaut P, Sarathy SM,Thomson MJ. A chemical kinetic study of n-butanol oxidation at elevated pressure in a jet stirred reactor. Proceedings of the Combustion Institute 2009;32:229-237.
47. Sarathy SM, Thomson MJ, Togbé C, Dagaut P, Halter F,Mounaim-Rousselle C. An experimental and kinetic modeling study of n-butanol combustion. Combustion and Flame 2009;156:852-864.
48. Britto Jr RF,Martins CA. Experimental analysis of a diesel engine operating in Diesel–Ethanol Dual-Fuel mode. Fuel 2014;134:140-150.
49. Heywood JB, *Internal Combustion Engine Fundamentals*1988, New York: McGraw-Hill.
50. Khan I, Greeves, G., and Wang, C. Factors affecting smoke and gaseous emissions from direct injection engines and a method of calculation. SAE Technical Paper 730169
51. Yao C, Zhang Z, Cheung C,Xu G. Experimental study on the effect of gaseous and particulate emission from an ethanol fumigated diesel engine. Science China Technological Sciences 2010;53:3294-3301.
52. Yao C, Cheung CS, Cheng C,Wang Y. Reduction of Smoke and NOx from Diesel Engines Using a Diesel/Methanol Compound Combustion System. Energy & Fuels 2007;21:686-691.
53. Raj CS, Arul S,Senthilvelan S. Some Comparative Performance and Emission Studies on DI Diesel Engine Fumigated with Methanol and Methyl Ethyl Ketone

Using Microprocessor Controlled Fumigator. The Open Fuels & Energy Science Journal 2008;1:74-78.
54. Cheung CS, Cheng C, Chan TL, Lee SC, Yao C,Tsang KS. Emissions Characteristics of a Diesel Engine Fueled with Biodiesel and Fumigation Methanol. Energy & Fuels 2008;22:906-914.
55. Zhang ZH, Cheung CS, Chan TL,Yao CD. Emission reduction from diesel engine using fumigation methanol and diesel oxidation catalyst. Science of The Total Environment 2009;407:4497-4505.
56. Janousek G. Evaluation of Ethanol and Water Introduction via Fumigation on Efficiency and Emissions of a Compression Ignition Engine Using an atomization technique. Biological Systems Engineering--Dissertations, Theses, and Student Research 2010;Paper 9:
57. Gilot P, Bonnefoy F, Marcuccilli F,Prado G. Determination of kinetic data for soot oxidation. Modeling of competition between oxygen diffusion and reaction during thermogravimetric analysis. Combustion and Flame 1993;95:87-100.
58. Neeft JPA, Nijhuis TX, Smakman E, Makkee M,Moulijn JA. Kinetics of the oxidation of diesel soot. Fuel 1997;76:1129-1136.
59. Dernaika B,Uner D. A simplified approach to determine the activation energies of uncatalyzed and catalyzed combustion of soot. Applied Catalysis B: Environmental 2003;40:219-229.
60. Stratakis GA,Stamatelos AM. Thermogravimetric analysis of soot emitted by a modern diesel engine run on catalyst-doped fuel. Combustion and Flame 2003;132:157-169.
61. Song J, Alam M,Boehman∗ AL. IMPACT OF ALTERNATIVE FUELS ON SOOT PROPERTIES AND DPF REGENERATION. Combustion Science and Technology 2007;179:1991-2037.
62. Rodríguez-Fernández J, Oliva F,Vázquez RA. Characterization of the Diesel Soot Oxidation Process through an Optimized Thermogravimetric Method. Energy & Fuels 2011;25:2039-2048.
63. Zhang D, Ma Y,Zhu M. Nanostructure and oxidative properties of soot from a compression ignition engine: The effect of a homogeneous combustion catalyst. Proceedings of the Combustion Institute 2013;34:1869-1876.
64. Agudelo JR, Álvarez A,Armas O. Impact of crude vegetable oils on the oxidation reactivity and nanostructure of diesel particulate matter. Combustion and Flame 2014;161:2904-2915.
65. Jaramillo IC, Gaddam CK, Vander Wal RL, Huang C-H, Levinthal JD,Lighty JS. Soot oxidation kinetics under pressurized conditions. Combustion and Flame 2014;161:2951-2965.
66. Wang C, Xu H, Herreros JM, Lattimore T,Shuai S. Fuel Effect on Particulate Matter Composition and Soot Oxidation in a Direct-Injection Spark Ignition (DISI) Engine. Energy & Fuels 2014;28:2003-2012.
67. Yehliu K, Vander Wal RL, Armas O,Boehman AL. Impact of fuel formulation on the nanostructure and reactivity of diesel soot. Combustion and Flame 2012;159:3597-3606.
68. Yehliu K, Armas O, Vander Wal RL,Boehman AL. Impact of engine operating modes and combustion phasing on the reactivity of diesel soot. Combustion and Flame 2013;160:682-691.

69. Vander Wal RL,Tomasek AJ. Soot oxidation: dependence upon initial nanostructure. Combustion and Flame 2003;134:1-9.
70. Ruiz MP, de Villoria RG, Millera A, Alzueta MU,Bilbao R. Influence of the temperature on the properties of the soot formed from C2H2 pyrolysis. Chemical Engineering Journal 2007;127:1-9.
71. Su DS, Jentoft RE, Müller JO, Rothe D, Jacob E, Simpson CD, et al. Microstructure and oxidation behaviour of Euro IV diesel engine soot: a comparative study with synthetic model soot substances. Catalysis Today 2004;90:127-132.
72. Boehman AL, Song J,Alam M. Impact of Biodiesel Blending on Diesel Soot and the Regeneration of Particulate Filters. Energy & Fuels 2005;19:1857-1864.
73. Al-Qurashi K,Boehman AL. Impact of exhaust gas recirculation (EGR) on the oxidative reactivity of diesel engine soot. Combustion and Flame 2008;155:675-695.
74. Seong HJ,Boehman AL. Impact of Intake Oxygen Enrichment on Oxidative Reactivity and Properties of Diesel Soot. Energy & Fuels 2011;25:602-616.
75. Seong HJ,Boehman AL. Studies of soot oxidative reactivity using a diffusion flame burner. Combustion and Flame 2012;159:1864-1875.
76. Seong HJ,Boehman AL. Evaluation of Raman Parameters Using Visible Raman Microscopy for Soot Oxidative Reactivity. Energy & Fuels 2013;27:1613-1624.
77. Setiabudi A, Makkee M,Moulijn JA. The role of NO2 and O2 in the accelerated combustion of soot in diesel exhaust gases. Applied Catalysis B: Environmental 2004;50:185-194.
78. Müller JO, Su DS, Jentoft RE, Wild U,Schlögl R. Diesel Engine Exhaust Emission: Oxidative Behavior and Microstructure of Black Smoke Soot Particulate. Environmental Science & Technology 2006;40:1231-1236.
79. Knauer M, Carrara M, Rothe D, Niessner R,Ivleva NP. Changes in Structure and Reactivity of Soot during Oxidation and Gasification by Oxygen, Studied by Micro-Raman Spectroscopy and Temperature Programmed Oxidation. Aerosol Science and Technology 2009;43:1-8.
80. Higgins KJ, Jung H, Kittelson DB, Roberts JT,Zachariah MR. Size-Selected Nanoparticle Chemistry: Kinetics of Soot Oxidation. The Journal of Physical Chemistry A 2001;106:96-103.
81. Higgins KJ, Jung H, Kittelson DB, Roberts JT,Zachariah MR. Kinetics of Diesel Nanoparticle Oxidation. Environmental Science & Technology 2003;37:1949-1954.
82. Jung H, Kittelson DB,Zachariah MR. The influence of a cerium additive on ultrafine diesel particle emissions and kinetics of oxidation. Combustion and Flame 2005;142:276-288.
83. Jung H, Kittelson DB,Zachariah MR. Characteristics of SME Biodiesel-Fueled Diesel Particle Emissions and the Kinetics of Oxidation. Environmental Science & Technology 2006;40:4949-4955.
84. Song J, Alam M, Boehman AL,Kim U. Examination of the oxidation behavior of biodiesel soot. Combustion and Flame 2006;146:589-604.
85. Vander Wal RL,Tomasek AJ. Soot nanostructure: dependence upon synthesis conditions. Combustion and Flame 2004;136:129-140.
86. Lee KO, Cole R, Sekar R, Choi MY, Kang JS, Bae CS, et al. Morphological investigation of the microstructure, dimensions, and fractal geometry of diesel particulates. Proceedings of the Combustion Institute 2002;29:647-653.

87. Zhu J, Lee KO, Yozgatligil A,Choi MY. Effects of engine operating conditions on morphology, microstructure, and fractal geometry of light-duty diesel engine particulates. Proceedings of the Combustion Institute 2005;30:2781-2789.
88. Lu T, Cheung CS,Huang Z. Effects of engine operating conditions on the size and nanostructure of diesel particles. Journal of Aerosol Science 2012;47:27-38.
89. Marsh H. A tribute to Philip L. Walker. Carbon 1991;29:703-704.
90. Salamanca M, Mondragón F, Agudelo JR, Benjumea P,Santamaría A. Variations in the chemical composition and morphology of soot induced by the unsaturation degree of biodiesel and a biodiesel blend. Combustion and Flame 2012;159:1100-1108.
91. Kuwahara T, Nishii S, Kuroki T,Okubo M. Complete regeneration characteristics of diesel particulate filter using ozone injection. Applied Energy 2013;111:652-656.
92. Gill SS, Tsolakis A, Herreros JM,York APE. Diesel emissions improvements through the use of biodiesel or oxygenated blending components. Fuel 2012;95:578-586.
93. Arenillas A, Rubiera F, Pevida C, Ania CO,Pis JJ. Relationship between structure and reactivity of carbonaceous materials. Journal of Thermal Analysis and Calorimetry 2004;76:593-602.
94. Santamaria A, Yang N, Eddings E,Mondragon F. Chemical and morphological characterization of soot and soot precursors generated in an inverse diffusion flame with aromatic and aliphatic fuels. Combustion and Flame 2010;157:33-42.
95. Iwashita N, Park CR, Fujimoto H, Shiraishi M,Inagaki M. Specification for a standard procedure of X-ray diffraction measurements on carbon materials. Carbon 2004;42:701-714.
96. Ergun S, Tiensuu, V.H. INTERPRETATION OF THE INTENSITIES OF X-RAYS SCATTERED BY COALS. Fuel 1959;38:64–78.
97. Agudelo JR, Álvarez A,Armas O. Impact of crude vegetable oils on the oxidation reactivity and nanostructure of diesel particulate matter. Combustion and Flame
98. SÁNCHEZ - VALDEPEÑAS J, *ESTUDIO DEL EFECTO DE LOS PARÁMETROS DE FUNCIONAMIENTO DE UN MOTOR DIÉSEL SOBRE LA REACTIVIDAD DEL HOLLÍN EMITIDO*, in *ESCUELA TÉCNICA SUPERIOR DE INGENIEROS INDUSTRIALES*2013, UNIVERSIDAD DE CASTILLA - LA MANCHA. p. 1-127.
99. Lapuerta M, Oliva F, Agudelo JR,Stitt JP. Optimization of Raman Spectroscopy Parameters for Characterizing Soot from Different Diesel Fuels. Combustion Science and Technology 2011;183:1203-1220.
100. Sadezky A, Muckenhuber H, Grothe H, Niessner R,Pöschl U. Raman microspectroscopy of soot and related carbonaceous materials: Spectral analysis and structural information. Carbon 2005;43:1731-1742.
101. Lapuerta M, Ballesteros R,Martos FJ. A method to determine the fractal dimension of diesel soot agglomerates. Journal of Colloid and Interface Science 2006;303:149-158.
102. Rakopoulos DC, Rakopoulos CD, Giakoumis EG, Dimaratos AM,Kyritsis DC. Effects of butanol–diesel fuel blends on the performance and emissions of a high-speed DI diesel engine. Energy Conversion and Management 2010;51:1989-1997.
103. Russo C, Stanzione F, Tregrossi A,Ciajolo A. Infrared spectroscopy of some carbon-based materials relevant in combustion: Qualitative and quantitative analysis of hydrogen. Carbon 2014;74:127-138.

104. Santamaría A, Mondragón F, Molina A, Marsh ND, Eddings EG,Sarofim AF. FT-IR and 1H NMR characterization of the products of an ethylene inverse diffusion flame. Combustion and Flame 2006;146:52-62.
105. Llamas-Jansa I, Jäger C, Mutschke H,Henning T. Far-ultraviolet to near-infrared optical properties of carbon nanoparticles produced by pulsed-laser pyrolysis of hydrocarbons and their relation with structural variations. Carbon 2007;45:1542-1557.
106. Russo C, Stanzione F, Tregrossi A, Alfè M,Ciajolo A. The effect of temperature on the condensed phases formed in fuel-rich premixed benzene flames. Combustion and Flame 2012;159:2233-2242.
107. Sukjit E, Herreros JM, Piaszyk J, Dearn KD,Tsolakis A. Finding Synergies in Fuels Properties for the Design of Renewable Fuels – Hydroxylated Biodiesel Effects on Butanol-Diesel Blends. Environmental Science & Technology 2013;47:3535-3542.
108. Gill SS, Herreros JM, Tsolakis A, Turner DM, Miller E,York APE. Filtered EGR - a step towards an improved NOX/soot trade-off for DPF regeneration. RSC Advances 2012;2:10400-10408.
109. Houser K, Lestz, S., Dukovich, M. and Yasbin, R. Methanol Fumigation of a Light Duty Automotive Diesel Engine. SAE Technical Paper 801379 1980;
110. Broukhiyan E,Lestz S. Ethanol Fumigation of a Light Duty Automotive Diesel Engine. SAE Technical Paper 1981;811209:
111. Heisey J,Lestz S. Aqueous Alcohol Fumigation of a Single-Cylinder DI Diesel Engine. SAE Technical Paper 1981;811208:
112. Singh P, DeMarini Dm Fau - Dick CAJ, Dick Ca Fau - Tabor DG, Tabor Dg Fau - Ryan JV, Ryan Jv Fau - Linak WP, Linak Wp Fau - Kobayashi T, et al. Sample characterization of automobile and forklift diesel exhaust particles and comparative pulmonary toxicity in mice. Environ Health Perspect. 2004;112:820-5.
113. Umbuzeiro GA, Franco A, Martins MH, Kummrow F, Carvalho L, Schmeiser HH, et al. Mutagenicity and DNA adduct formation of PAH, nitro-PAH, and oxy-PAH fractions of atmospheric particulate matter from São Paulo, Brazil. Mutation Research/Genetic Toxicology and Environmental Mutagenesis 2008;652:72-80.
114. Noble PB,Cutts JH. Separation of blood leukocytes by Ficoll gradient. Can Vet J. 1967;8:110-1.
115. Mendoza LC, Orozco LY, Zapata LM,Palacio JA. Genotoxicidad sobre linfocitos humanos expuestos a PM10 de tres sitios del Valle de Aburrá (Antioquia). Revista de Salud Pública 2013;12:294-306.
116. Platel A, Gervais V, Sajot N, Nesslany F, Marzin D,Claude N. Study of gene expression profiles in TK6 human cells exposed to DNA-oxidizing agents. Mutation Research/Fundamental and Molecular Mechanisms of Mutagenesis 2010;689:21-49.
117. Zúñiga LA, *Optimizaciones metodológicas del ensayo del cometa y su aplicación en biomonitorización humana*, 2009, Universitat Autònoma de Barcelona. Departament de Genètica i de Microbiologia. p. 223.
118. Singh NP, McCoy MT, Tice RR,Schneider EL. A simple technique for quantitation of low levels of DNA damage in individual cells. Experimental Cell Research 1988;175:184-191.
119. McNamee JP, McLean JRN, Ferrarotto CL,Bellier PV. Comet assay: rapid processing of multiple samples. Mutation Research/Genetic Toxicology and Environmental Mutagenesis 2000;466:63-69.

120. Rodriguez Ferreiro G, Cancino Badías L, Lopez-Nigro M, Palermo A, Mudry M, González Elio P, et al. DNA single strand breaks in peripheral blood lymphocytes induced by three nitroimidazole derivatives. Toxicology Letters 2002;132:109-115.

7. ANNEXES

7.1 ANNEX 1: Electronic Control Unit of Alcohols

Electronic control unit (ECU) of alcohols is responsible to management and control of ethanol injection in the diesel engine. ECU is divided in two part: the first part is responsible to configure the injection time and the second is in charge to supply the energy of the injector. Control stage is composed for a Freescale™ microcontroller and some operational amplifier; the microcontroller is the brain of ECU and receive all signals sensor, also it is that dictates injection duration and when the injection occurs (Fig. 27).

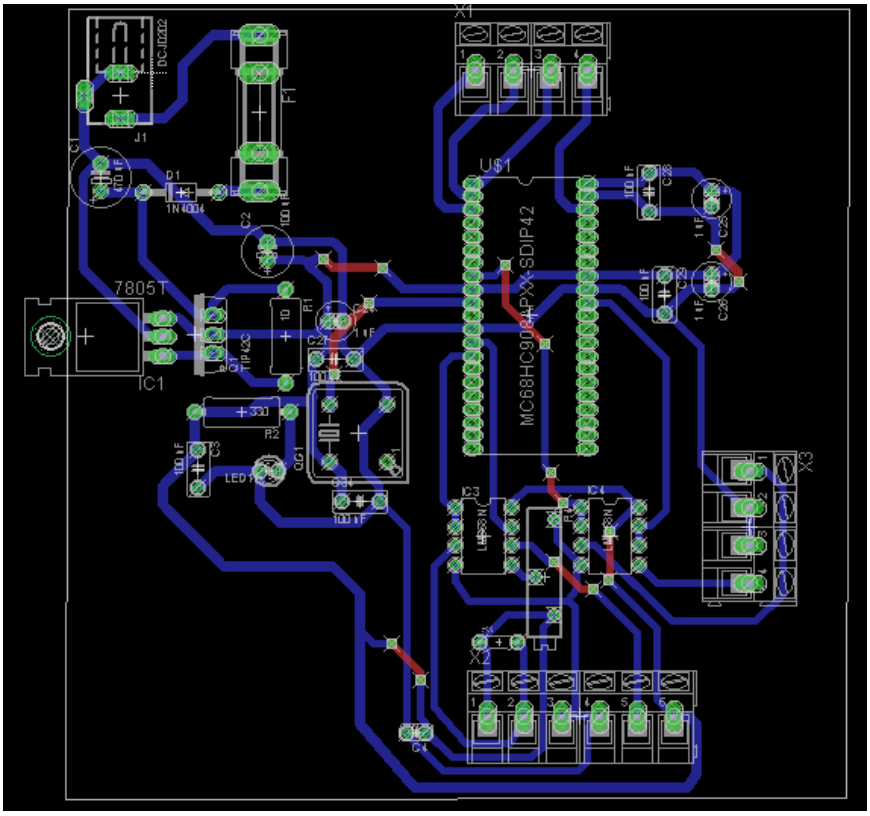

Fig. 27 Control stage ECU

In the control stage was installed two sensors in the diesel engine. A sensor of proximity was installed in inlet valve of the cylinder 1 to determine top dead center (TDC) intake and rpm sensor which sends 60 pulses per revolution was mounted in the crankshaft (Fig. 28).

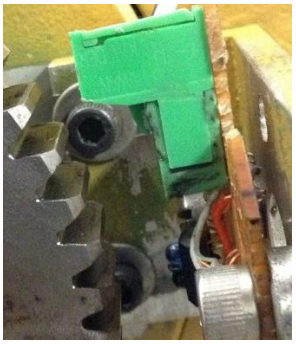

Fig. 28 Sensors of TDC and rpm

Supply stage (Fig. 29) was implemented with DC-DC converters, which were implemented with N-MOSFET transistors. This stage is responsible for ensuring the current for the correct operation of injectors

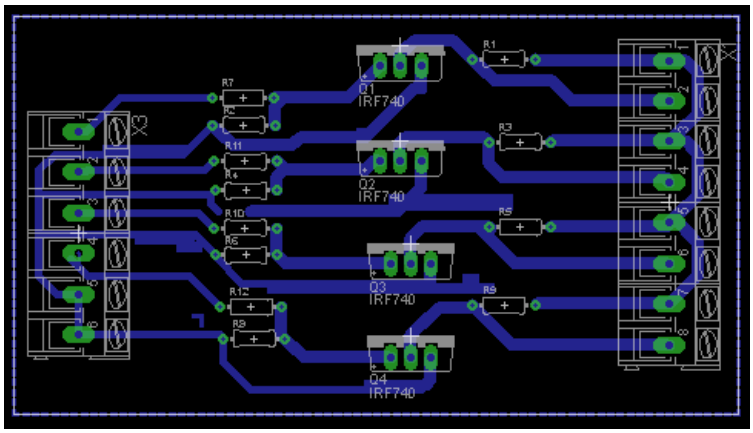

Fig. 29 Supply stage

7.1.1 Algorithm of alcohols fumigation

The algorithm of alcohols fumigation (Fig. 30) was implemented in a Freescale™ microcontroller and Labview™ software (Fig. 31). The first step of the algorithm was configure the initial parameters for the correctly operation of microcontroller; later the algorithm read the injector opening time from the Labview-based software. The next step was to find top dead center (TDC) of intake in the cylinder 1, with this signal can be referenced and synchronize the injection in all injectors. Then, the algorithm received the pulses of rpm signal and each 30 pulses going to enable the injector should fumigate, the sequence the fumigation is 2-3-4-1, in each cylinder respectively

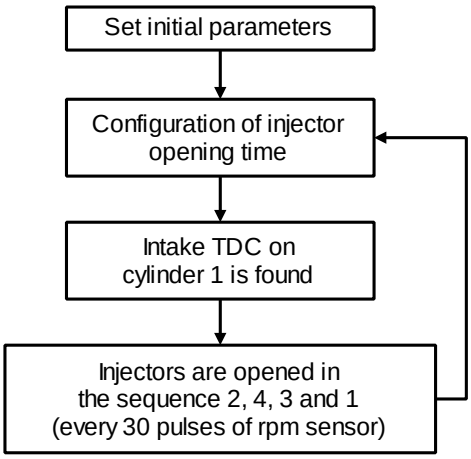

Fig. 30. Algorithm alcohol injection

Fig. 31 Labview interfaz

7.2 ANNEX 2: Injector Characterization

All injectors were characterized to determine if they injected the same amount of alcohols (Fig. 32). For characterization was used the method of difference of weight to same injection time, the Table 11 show the injection time that was characterized and the number of injections per injector.

Fig. 32. Calibration system

Table 11. Time of characterization of the injector

Injection time (ms)	Number of pulse per injectors
20	225
10	300
5	400
3	1000
2	1250

The result of characterzation are show in the Fig. 33: The minimum time opening of injector was to 1.5 ms, that is the time necessary of suply to energy of injector.

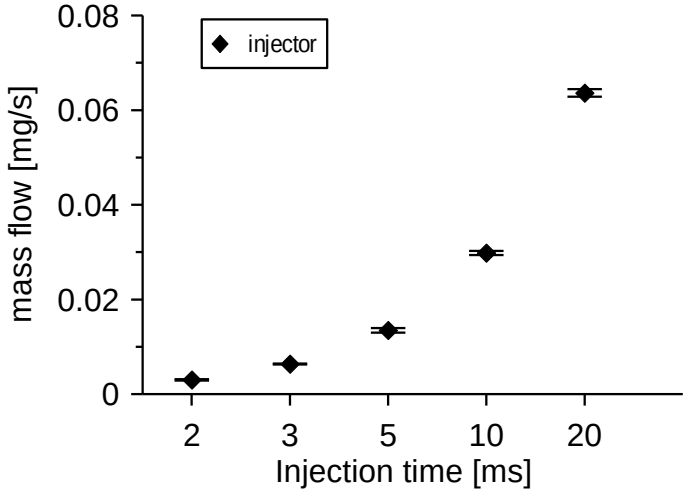

Fig. 33 Mass flow characterization

7.3 ANNEX 3. Economic Analysis

Economic analysis was realized with basis of current price of diesel and ethanol in Colombia and Brazil (see Table 12). In this study was assumed that the thermal efficiency was equal regardless of the substitution of alcohol, and depending on the low heating value

Table 12. Fuel prices

Fuel	Colombia (US$/litro)	Brazil (US$/litro)
Diesel	1.06 [(b)]	1.03 [(b)]
Ethanol hydrated (Et-h)	----	0.4713 [(a)]
Ethanol anhydrous (Et-a)	0.82 [(c)]	0.5382 [(a)]

(a) Centro de Estudos Avançados em Economia Aplicada http://cepea.esalq.usp.br/etanol. Visited on 23 October 2014

(b) http://es.globalpetrolprices.com/diesel_prices. Visited on 23 October 2014

(c) Federación de biocombustibles de Colombia http://www.fedebiocombustibles.com/v3 . Visited on 23 October 2014

Fig. 34 shows infeasibility to use of ethanol fumigation in Colombia, this is because the ethanol price in Colombia is very expensive compared with Brazil. A possible implementation of fumigation in Colombia is in the sugarmill of Valle del Cauca, where save the cost of transport.

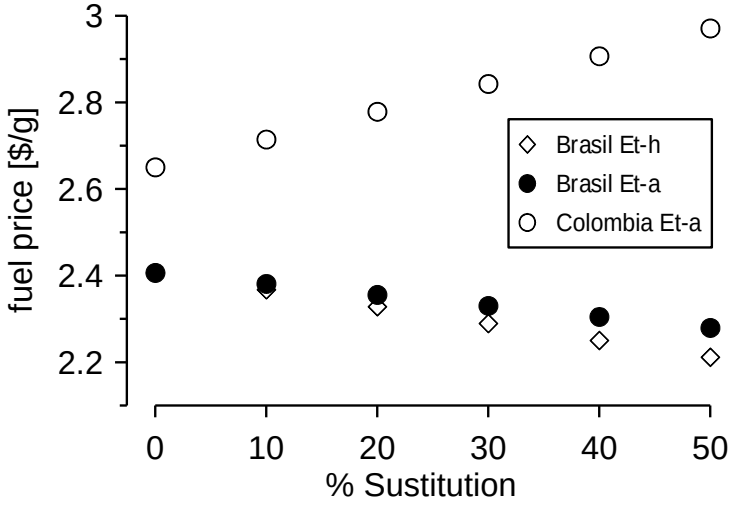

Fig. 34 Economic analysis

7.4 ANNEX 4. Genotoxic assessment table

			%V	X ± SD [µm]	%DC	WDI
Control	Negative	PBS	100	7 ± 2	3	10
	Positive	H_2O_2	75	52 ± 13	100	688
	Solvent	DMSO	98	8 ± 2	5	15
µg-eq PM	**Mode**	**Fuel**				
8	M2	ULSD	100	8 ± 2	7.3	22
		n-Bu10	100	9 ± 3	21	63
		H-Et10	100	9 ± 3	29	86
	M4	ULSD	100	7 ± 1	6	17
		n-Bu10	100	9 ± 2	35	104
		H-Et10	90	23 ± 7	94	313
16	M2	ULSD	100	8 ± 2	8.3	25
		n-Bu10	100	9 ± 3	34	103
		H-Et10	100	14 ± 5	65	195
	M4	ULSD	100	8 ± 3	15	46
		n-Bu10	100	10 ± 3	42	126
		H-Et10	83	29 ± 9	96	394
31	M2	ULSD	100	9 ± 2	13	39
		n-Bu10	100	12 ± 5	55	164
		H-Et10	95	15 ± 6	72	217
	M4	ULSD	100	10 ± 4	36	108
		n-Bu10	96	13 ± 4	67	201
		H-Et10	81	36 ± 8	100	463
63	M2	ULSD	100	11 ± 3	42	168
		n-Bu10	94	15 ± 4	78	235
		H-Et10	95	19 ± 8	83	261
	M4	ULSD	96	17 ± 7	71	213
		n-Bu10	93	18 ± 5	91	272
		H-Et10	81	42 ± 10	100	528
125	M2	ULSD	100	12 ± 4	56	168
		n-Bu10	84	17 ± 7	77	236
		H-Et10	90	31 ± 11	97	391
	M4	ULSD	94	18 ± 6	91	274
		n-Bu10	89	24 ± 8	100	298
		H-Et10	77	48 ± 12	100	630
250	M2	ULSD	96	23 ± 9	88	300
		n-Bu10	75	26 ± 13	92	335
		H-Et10	80	44 ± 10	100	552
	M4	ULSD	92	28 ± 8	98	357
		n-Bu10	88	31 ± 7	100	403
		H-Et10	76	51 ± 12	100	656
500	M2	ULSD	92	27 ± 10	91	334
		n-Bu10	75	40 ± 15	99	485
		H-Et10	76	49 ± 13	100	645
	M4	ULSD	82	40 ± 8	100	521
		n-Bu10	81	44 ± 12	100	569
		H-Et10	75	54 ± 11	100	708